ICE SCALING IN CONTINUOUS EUTECTIC FREEZE CRYSTALLIZATION

Debora Jooste

Dissertation submitted in partial fulfilment of the requirements for the degree of Master of Science in Engineering

---

Department of Chemical Engineering

Faculty of Engineering and Built Environment

University of Cape Town

February, 2016

***Declaration*:** *I know the meaning of plagiarism and declare that all the work in the document, save for that which is properly referenced, is mine*

.....

Acknowledgements

I would like to thank the following people and authorities:

Prof Alison Lewis, supervisor of this study, who provided support, advice and guidance. Your knowledge of crystallization and especially eutectic freeze crystallization proved to be invaluable during the research process.

Mr Jemitias Chivavava, co-supervisor of this study, my sincere thanks for your assistance and guidance. Your attention to detail and endless enthusiasm for the work is appreciated.

Mrs Hayley Battle, thank you for your assistance as part of the Crystallization and Precipitation team. To my fellow students, Chiara, Senzo and Cledwyn, thank you for your input and assistance.

The Water Research Commission is acknowledged for making this research possible.

Finally, thanks to my partner, Robert, and my parents for allowing me the belief that I could successfully complete this journey.

Abstract

Eutectic Freeze Crystallization (EFC) is a novel and potentially cost effective technique to treat industrial brines by the simultaneous crystallization of ice and salt under sub-eutectic conditions. Previous research has demonstrated that the formation of an ice scale layer on the cooling surfaces of indirectly cooled crystallizers severely decreases heat transfer. This increases the mechanical energy requirements and overall operational cost of the process. The energy efficiency of EFC as a wastewater treatment and resource recovery technology is, therefore, dependent on effective control of ice scaling. This research focused on determining the induction time, defined as the time between initial nucleation and scale layer formation, where shorter induction times are associated with more severe scaling tendencies. The experimental work was conducted in a hybrid crystallizer-separator with a 2 litre crystallization zone fitted with a mechanical scraping device. The effect of the driving force for heat transfer, scraper speed and the solute type and concentration of inorganic electrolyte impurities in a binary eutectic Na_2SO_4-H_20 system was investigated. Induction time decreased with an increase in the driving force for heat transfer, due to a lower wall temperature and an increased driving force for crystallization as a result of the higher heat flux. An increase in scraper speed resulted in an increase in induction time, due to the more frequent removal of the thermal boundary layer and better distribution of supersaturation and magma throughout the crystallizer. The induction time was found to be specific to dissolved ionic species as a result of unique electrostatic interactions between the cooled wall and ice layer surface. Induction time showed an increase with an increase in concentration of electrolyte impurities, due to the increased mass transfer limitation of solute molecules away from the growing ice front.

Contents

Figures

Tables

Nomenclature

a	Activity	kg/kg solvent
a^*	Equilibrium activity	kg/kg solvent
A	Surface area	m^2
b	Exponent	
C	Solute concentration	kg/kg solvent
C_p	Specific heat capacity	J/kg^oC
C*	Solubility or equilibrium concentration	kg/kg solvent
c	Exponent	
D	Impeller diameter	m
d	Particle size	m
E	Dimensionless constant	
e	Positive integer	
F	Number of scraper blades	
g	Gravitational acceleration	m/s^2
J	Nucleation rate	$nuclei/m^3s$
K	Dimensionless constant	
K_{pen}	Penetration theory correction factor	
k_B	Boltzmann constant	J/K
L	Characteristic length	m
m	Mass	kg

$\dot{m}$	Mass flow rate	kg/s
N	Impeller speed	rev/s
n	Rotational speed	rpm
Q_{ice}	Heat of crystallization of ice	W
Q_{feed}	Sensible heat of feed stream	W
Q_{loss}	Heat loss to environment	W
Q_{cm}	Heat absorbed by cooling medium	W
Q_{salt}	Heat of crystallization of salt	W
S	Dimensionless constant	
S_r	Supersaturation ratio	
T	Temperature	^oC
T*	Equilibrium temperature	°C
U_o	Overall heat transfer coefficient	W/m^2°C
W	Dimensionless constant	
X	Solids mass fraction	

Dimensionless numbers

Nu	Nusselt
Pr	Prandtl
Re	Reynolds

Greek symbols

σ	Relative supersaturation	
μ	Chemical potential	J/kg
μ^*	Chemical potential at equilibrium	J/kg
ν	Kinematic viscosity	m^2/s
ν_m	Molecular volume	m^3/mol
λ	Thermal conductivity	W/m°C
γ_s	Shear rate	N/m^2
τ	Time between scraper passes	s
τ_s	Shear stress	N/m^2
ρ	Density	kg/m^3
ρ_m	Magma density	kg/m^3 of slurry
δ	Thickness	m
α	Heat transfer coefficient	W/m^2°C
π	Mathematical constant	3.142
η	Fluid viscosity	P
θ	Wetting angle	degrees

1 Introduction

1.1 Background

South Africa is a mineral rich, but water scarce country, with a growing population. The Bushveld complex contains an estimated 95 % of the global platinum group metal (PGM) reserves, with production of PGM's from South Africa representing 48 % of the worldwide total in 2014. Gold deposits, primarily found in the Witwatersrand, represent 11 % of global reserves, while significant quantities of manganese, diamonds, chromite ore and vanadium are also mined in South Africa (US Geological Survey, 2015). Processing of minerals requires large amounts of water, with estimations for gold processing at 5000 litres of water per ounce of gold (Cloete, Gerber & Maritz, 2010). Processing operations produce wastewater containing dissolved salts, however, the leading environmental concern associated with mining operations is acid mine drainage (AMD), which occurs when water comes into contact with sulphur bearing rock, such as pyrite, to produce a highly acidic water stream.

Although South Africa boasts a variety of climatic zones, the majority of the country is arid, with the annual average precipitation being 495 mm, less than half the annual global average of 1033 mm (World Bank Database, 2015a). Renewable water resources per capita in South Africa are estimated at 843 m^3/inhabitant·year, low in comparison to the availability of renewable water resources in the USA, an order of magnitude higher at 8904 m^3/inhabitant·year (World Bank Database, 2015b). Putting further strain on an already limited fresh water supply is a population growth rate of approximately 1.5 % per year (Statistics South Africa, 2015).

In view of the high demand for fresh water from both industrial and municipal users, treatment of wastewater has become increasingly important. Several technologies exist to treat acidic water streams and wastewater containing dissolved salts; these are summarized in Figure 1.1. The first step in the treatment of AMD is neutralization of the highly acidic water. Neutralization processes, shown in Figure 1.1, produce sludge and water as products, with both streams typically of a quality that needs further treatment to allow beneficial use (Johnson & Hallberg, 2005). Removal of salts from the neutralized AMD water stream, as well as from wastewater originating from minerals processing plants, can be achieved by a combination of reverse osmosis and crystallization processes. During these salt removal

processes, shown in Figure 1.1, the volume of wastewater is reduced and potable water is produced together with a concentrated brine stream (Gunther & Naidu, 2008). The residual brine stream now contains the salts at high concentrations, limited by the solubility of each species.

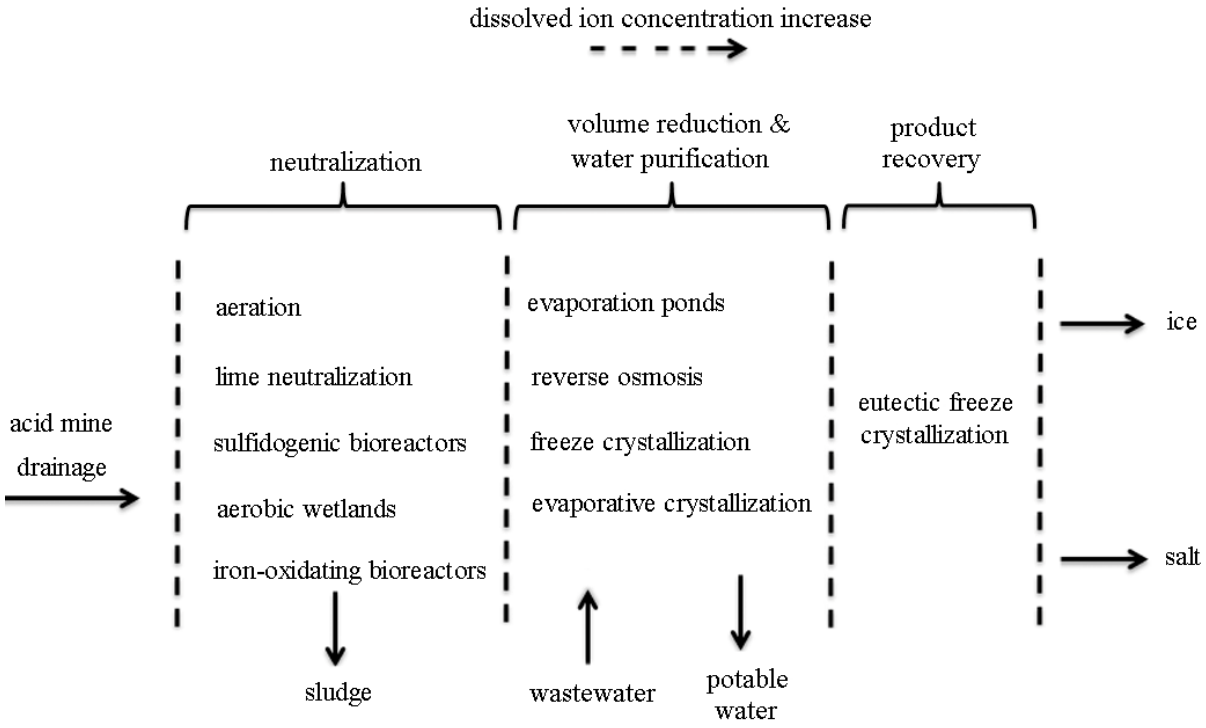

Figure 1.1: Process options for AMD and wastewater treatment

Eutectic freeze crystallization (EFC) is a novel water treatment technology, which allows recovery of ice and salt products from a concentrated brine stream, as shown in Figure 1.1. The use of EFC as part of the overall water treatment process holds several advantages. As crystallization is a physical separation process, it does not require the addition of chemical substances (Lorain et al., 2001). Freeze crystallization is thermodynamically more efficient than evaporative crystallization, as the heat of fusion of water is six times lower than the heat of evaporation of water (Van der Ham, 1999). Under eutectic conditions, ice and salt crystallize simultaneously and can be separated based on density differences (Genceli, 2008). Crystallization of both products occurs in pure form, eliminating the need for a secondary separation process (Halde, 1980). A significant percentage of the energy used to achieve low operating temperatures is stored in the ice product and can be recovered. Low operating temperatures further reduce the potential for corrosion of mechanical equipment, allowing the use of less expensive construction materials (Johnson, 1976). Disadvantages of EFC include

high capital costs (Randall, 2010) and the formation of an insulating ice scale layer on cooled crystallizer surfaces (Pronk, 2006).

1.2 Project aim and scope of work

The aim of this project was to investigate the phenomenon of ice scale formation under eutectic conditions, in order to inform future design and operation of indirectly cooled continuous crystallization systems. The work forms part of a research theme on EFC which has been underway at the University of Cape Town for almost a decade. The development of continuous EFC systems for application to wastewater treatment in the mining and minerals processing sectors in South Africa is one of the key objectives within this research theme.

The scope of this project included investigation of crystallizer operating conditions and the nature of the wastewater stream on the onset time for the formation of an ice scale layer. Employing a jacketed, scraped wall crystallizer, the effects of the driving force for heat transfer across the crystallizer wall and the rotational speed of the scrapers were investigated. An aqueous, binary sodium sulphate solution was used as the basis for investigation and the effects of the addition of several impurities at varying concentrations on the onset time for scaling were determined.

1.3 Thesis outline

Chapter 2 of this thesis provides the basic theory necessary to understand crystallization, eutectic freeze crystallization and heat transfer in scraped wall crystallizers. The theory behind the factors that influence scale formation is also included. In Chapter 3, the project is put into perspective by a discussion of relevant literature available on the factors influencing scale formation as well as a brief history of problems experienced due to ice scaling. The context and motivation for this project is given in Chapter 4. Chapter 5 outlines the methodology employed in the experimental work, including the experimental design, setup and procedure. The experimental results as well as a thorough discussion thereof are given in Chapter 6. Conclusions are drawn in Chapter 7 and Chapter 8 provides a few recommendations for future work.

2 Theory

2.1 Crystallization

The process of crystallization involves a phase change in which a solid forms from a supersaturated liquid solution melt or vapour. Supersaturation is defined as the thermodynamic driving force for the formation of the solid phase and the phase change is thermodynamically favoured when the Gibbs free energy of the transformation is less than zero (Dirksen & Ring, 1991). The relative supersaturation (σ) is an indication of how far the solution has deviated from thermodynamic equilibrium and can be expressed in terms of chemical potential (μ), activity (a) or temperature (T), as shown by Equations 2.1 to 2.3, where the asterisk denotes the equilibrium condition (Ulrich & Stelzer, 2011):

$$\sigma = \frac{\mu - \mu^*}{\mu^*} \tag{2.1}$$

$$\sigma = \frac{a - a^*}{a^*} \tag{2.2}$$

$$\sigma = \frac{T^* - T}{T^*} \tag{2.3}$$

Supersaturation can be referred to as undercooling when it is achieved through application of a temperature difference. Assuming that the activity coefficient has a value of unity, Equation 2.2 can be rewritten in terms of concentration (C), a quantity which can be measured with ease.

$$\sigma = \frac{C - C^*}{C^*} \tag{2.4}$$

2.2 Eutectic phase diagrams

Supersaturation can be graphically represented on a phase diagram, as shown for the binary aqueous sodium sulphate system in Figure 2.1. Phase diagrams depict the thermodynamically stable phases within a range of temperature and composition combinations (Mullin, 2001). Where a gaseous phase is present, pressure has an influence on the thermodynamics, but this

is not applicable to the solid-liquid transformations of aqueous electrolyte systems during cooling crystallization.

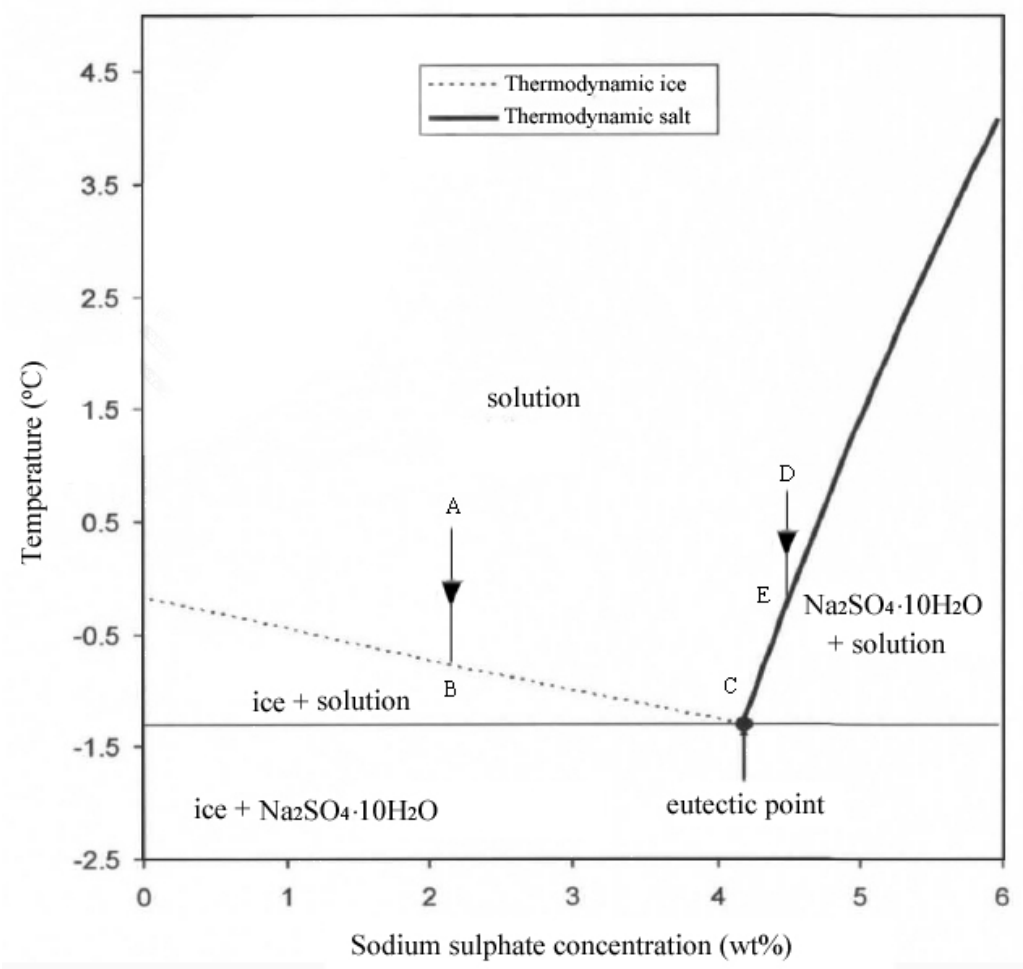

Figure 2.1: Binary eutectic phase diagram for the aqueous sodium sulphate system (Thomsen, 1997)

During a batch process, cooling a dilute solution from point A to point B (Figure 2.1) will result in the crystallization of ice. Upon further cooling ice will continue to crystallize, concentrating the solution, until the eutectic point is reached at C. For crystallization to occur, a small supersaturation must be maintained which will result in the cooling curve being slightly below the equilibrium line. For concentrated solutions, cooling from point D to point E will result in the crystallization of sodium sulphate decahydrate which will continue to crystallize out upon subsequent cooling to point C. At the eutectic point, further cooling will create a supersaturation with respect to both ice and salt, and simultaneous crystallization will occur while the concentration of the residual solution remains constant. Crystallization occurring under eutectic conditions, where both solvent and solute crystals are produced, is called eutectic freeze crystallization (EFC). During a continuous process, the operating point

remains constant once steady state is reached, which for EFC is just below the equilibrium point, C.

The thermodynamic behaviour of three-component systems can be graphically represented with the use of ternary phase diagrams. Several two and three dimensional methods exist to depict these diagrams, one of which is shown in Figure 2.2. In Figure 2.2, composition is represented along the sides of the triangle, while the dotted lines represent isotherms. The binary eutectic points are represented by the solid lines extending inward, and meet at the ternary eutectic point; C. Cooling the solution along line DC will result in the crystallization of salt A and ice, concentrating the residual solution with regard to salt B. Further cooling will result in crystallization of all three components, while the concentration of the residual solution remains constant.

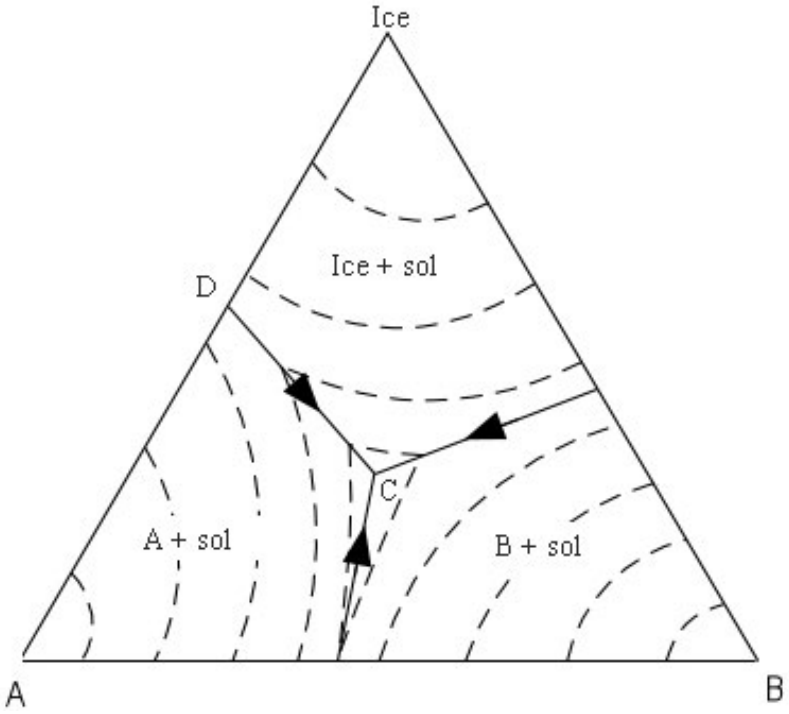

Figure 2.2: Theoretical ternary phase diagram (Nelson, 2011)

2.3 Crystallization processes

Crystallization processes are influenced not only by the thermodynamic properties of a system, as depicted in phase diagrams, but also, to a very large extent, by its kinetics. Nucleation, growth and the metastable zone width are important kinetic properties of any crystallization process.

2.3.1 **Nucleation**

Nucleation is the process of random generation of nanoscopically small formations of the new crystalline phase that reach a critical size, from which irreversible growth to macroscopic sizes is possible (Kashchiev, 2000). A distinction is made between primary and secondary nucleation of which primary nucleation is further subdivided into homogeneous and heterogeneous.

2.3.1.1 Primary nucleation

Primary nucleation occurs spontaneously once the upper limit of the metastable zone is reached. Homogeneous primary nucleation refers to the formation of new crystalline particles within a solids-free solution while heterogeneous primary nucleation refers to the formation of new crystalline particles on a solid surface within the crystallizer, such as the walls of the vessel, the mixing equipment, dust particles or solid impurities in solution.

The nucleation rates of homogeneous and heterogeneous primary nucleation differ, where heterogeneous nucleation is substantially faster, due to the prior existence of a surface which reduces the crystalline surface area required to form during the nucleation step. The homogeneous and heterogeneous nucleation rates are given by Equations 2.5 and 2.6 (Mullin, 2001):

$$J_{hom} = E_{hom}\exp(-\frac{16\pi\gamma^3 v_m^2}{3T^3 k_B^3 (lnS_r)^2}) \quad 2.5$$

$$J_{het} = E_{het}\exp(-\frac{16\pi\gamma^3 v_m^2 f(\theta)}{3T^3 k_B^3 (lnS_r)^2}) \quad 2.6$$

where E is a pre-exponential factor, γ is the interfacial surface tension, v_m is the molecular volume, T is the temperature, k_B is the Boltzmann constant and S_r is the supersaturation ratio. During heterogeneous nucleation, the contact angle between the existing surface and the newly formed crystal surface is termed the wetting angle (θ), which can range between 0° and 180°. In Equation 2.6 above, $f(\theta)$ is a geometric factor ranging between 0 and 1, as defined in Equation 2.7 (Mullin, 2001):

$$f(\theta) = \frac{(2 + cos\theta)(1 - cos\theta)^2}{4} \quad 2.7$$

2.3.1.2 Secondary nucleation

Secondary nucleation refers to the formation of new crystalline particles, either in the vicinity of existing particles of the same crystalline nature, or through interparticle collisions. The rate of secondary nucleation is higher than that of primary nucleation due its lower energy requirements (primary homogeneous < primary heterogeneous < secondary), and it is therefore the dominant form of nucleation in continuous crystallization processes. The secondary nucleation rate is a complex function of the magma density, supersaturation and fluid dynamics within a crystallization vessel (Mullin, 2001). A widely accepted approximation for the secondary nucleation rate within stirred vessels is given by Equation 2.8 (Hossein & Da-Wen, 2011):

$$J_{sec} = K\rho_m^j N^h \sigma^p \qquad 2.8$$

where K is a nucleation constant, ρ_m is the magma density, N is the agitator speed and σ is the supersaturation, with the respective exponents, j, h and p showing the order of dependence.

2.3.2 **Metastable zone**

The metastable zone comprises an area on the phase diagram below the equilibrium line, in which nucleation is kinetically limited to primary heterogeneous and secondary nucleation (Ulrich & Jones, 2006). The addition of parent crystals to the crystallizer, in order to initiate nucleation within the metastable zone, is called seeding and is a method used to control crystal size and morphology.

2.3.3 **Growth**

Crystal growth can be described simply as the adsorption and subsequent incorporation of lattice units onto an existing crystal surface. Defining the growth rate for crystals growing in suspension is, however, slightly more complex as each crystalline face grows at its own rate. The overall linear growth rate is usually described as a combined function of the increase in specific crystal mass and the linear growth rates in the direction normal to each crystalline face (Lewis et al., 2015).

2.3.3.1 Ice layer growth

The description of the growth rate is simplified in the case of growth on a solid surface such as a crystallizer wall. After initial nucleation, a short period of lateral growth occurs during

which the wall is covered in a very thin film of ice (Qin, Chen & Farid, 2004). Planar growth, in the direction normal to the wall, then ensues which involves three steps. Water molecules must be incorporated into the crystal lattice, salt molecules must diffuse away from the growing ice front and the heat of crystallization must be removed to maintain supersaturation (Myerson & Ginde, 2002). These processes are graphically shown in Figure 2.3, where δ_d is the thickness of the diffusion boundary layer.

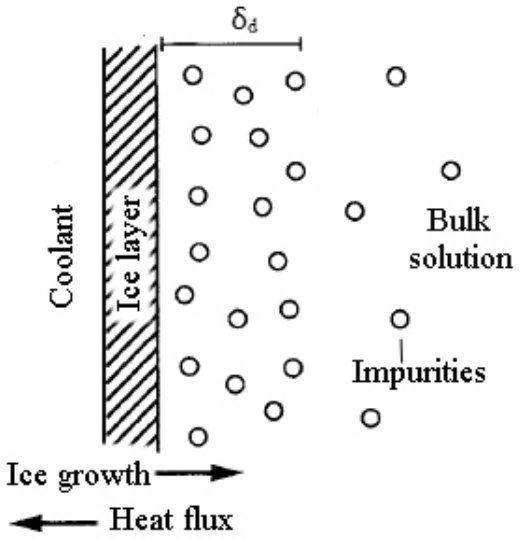

Figure 2.3: Ice layer growth on a cooled surface (Myerson & Ginde, 2002).

Depending on the process characteristics, any one of the three steps involved in crystal growth could be the rate limiting step. Melt crystallization is distinguished from solution crystallization based on the nature of the crystallizing component and, therefore, the relative contributions of mass and heat transfer toward the resistance to crystal growth (Mersmann, 2001). During melt crystallization, the solvent is the crystallizing component and the removal of heat of crystallization from the growing crystal front is the rate limiting process. The heat of crystallization can be transferred to both the bulk solution and the existing crystal surface. In the case of ice layer growth on a cooled surface, as shown in Figure 2.3, the majority of the heat is conducted through the existing ice layer since the ice is in contact with the cooled surface (Pronk, 2006). During solution crystallization, the solute is the crystallizing component and the diffusion of molecules toward the growing crystal surface limits the growth rate. The process is; therefore, mass transfer controlled (Mersmann, 2001). Eutectic freeze crystallization involves a combination of both melt and solution crystallization, as ice and salt form under eutectic conditions. Ice layer growth can, therefore, be either mass or heat transfer controlled.

The rate of incorporation of water molecules into the crystal lattice is a kinetic property specific to each system. In aqueous electrolyte solutions, the presence of solute molecules can affect incorporation kinetics through adsorption on the ice surface and by influencing the movement of water molecules at the ice-liquid interface (Huige, 1972). The overall rate of ice layer growth is strongly dependent on the average local supersaturation at the solid-liquid interface and any change in process variables, which affect this local supersaturation, has a major effect on ice layer formation on cooled crystallizer surfaces, otherwise known as ice scale formation.

2.4 Ice scaling

During suspension crystallization of electrolyte solutions, where indirect cooling is applied, conditions that favour the formation of an ice scale layer on cooled heat exchanger surfaces are created. The conductivity of ice is several times smaller than that of materials that are typically used for the construction of crystallization vessels. An ice scale layer, therefore, increases thermal resistance and decreases the heat removal rate from the suspension, adversely affecting the production rates of ice and salt in an EFC process.

The formation of this ice scale layer can be particularly severe due to the surface that is provided for heterogeneous nucleation, the large temperature driving forces that are applied across the surface to promote high production rates and the electrolyte solutions that typically consist of more than 80 % water which is, in this case, the scalant. Furthermore, any mechanical equipment within the crystallizer serves as additional surfaces for adhesion and ice growth.

2.4.1 Surface area for heterogeneous nucleation

The free energy of formation of nanoscopic particles of critical size is smaller for heterogeneous nucleation than for homogeneous nucleation because the surface area that must form between the new solid phase and the liquid solution is reduced during heterogeneous nucleation (Fletcher, 1958). Therefore, when a supersaturated solution is in contact with a solid surface, heterogeneous nucleation will occur in preference to homogeneous nucleation. In contrast to homogeneous nucleation, heterogeneous nucleation is not colligative; the heterogeneous nucleation rate depends not only on the ratio of the number of solute particles to solvent particles, but also on the nature of the solute (Koop et al., 2000).

2.4.2 **Thermal boundary layer**

Crystallizer walls experience the lowest temperature within the crystallizers since their externals are in thermal contact with the coolant flowing through the jacket. A thermal boundary layer develops between the wall and the bulk liquid, as depicted in Figure 2.4(a). The stagnant solution adjacent to the wall surfaces is, therefore, at a higher supersaturation than the bulk. This high local supersaturation prompts excessive heterogeneous nucleation and growth of an ice scale layer on the heat exchanger surface as noted by Pronk (2006); see Figure 2.4(b).

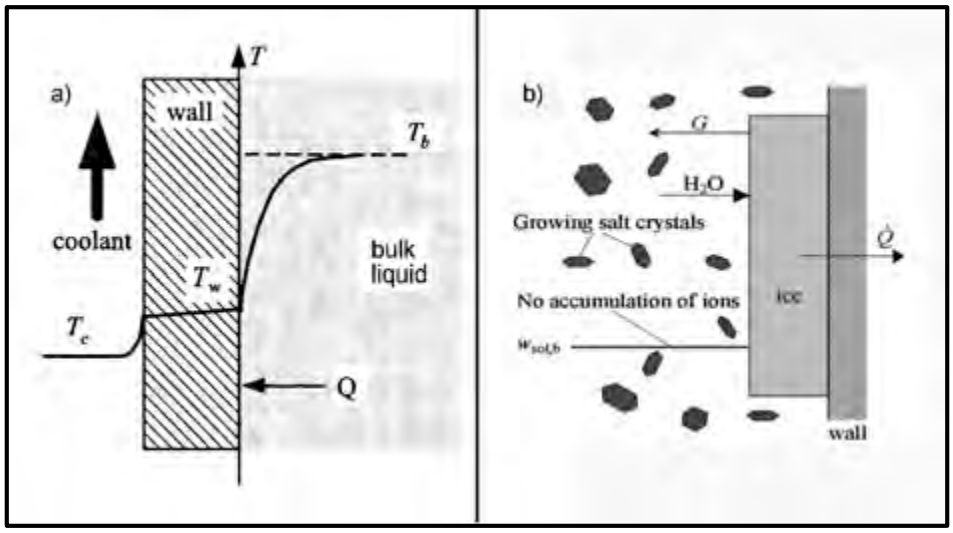

Figure 2.4: (a) Temperature profile promoting scale formation (Qin, Chen & Russell, 2003) (b) scale formation during EFC (Pronk, 2006)

Two main crystallizer configurations have been researched with the aim of combatting scale formation. In a fluidized bed configuration, metal particles are used to mechanically remove ice from the crystallizer walls during fluidization (Pronk, 2006). Alternatively, a scraped wall crystallizer has been used, where each scraper pass removes the thermal boundary layer as well as any crystals that have formed on the surface. The boundary layer develops again rapidly after each pass, as shown in Figure 2.5, and the average temperature over a complete scrape cycle remains colder at the surface than in the bulk liquid.

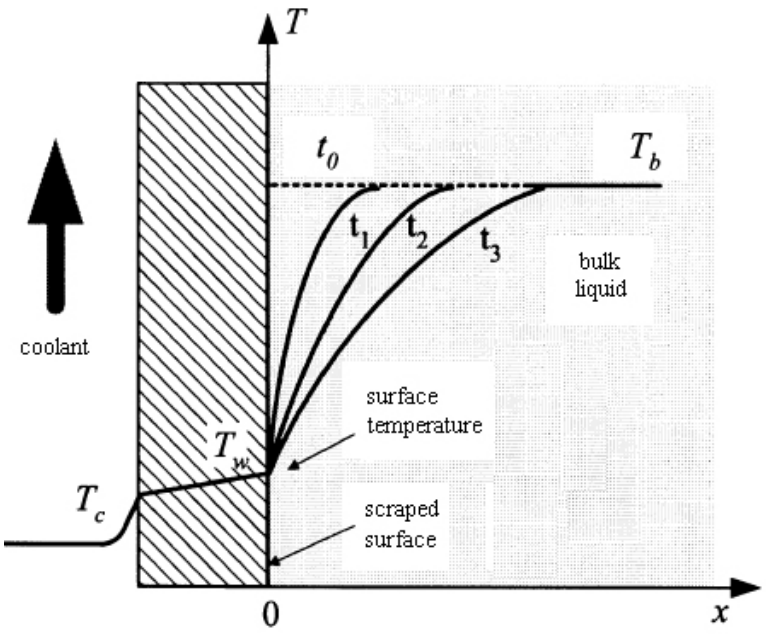

Figure 2.5: Development of the thermal boundary layer after each scraper pass (Qin et al., 2003)

In cylindrical crystallization vessels, where rotational scraping devices are used, the time between consecutive scraper passes is given by Equation 2.9 :

$$\tau = \frac{60}{nF} \qquad 2.9$$

where n is the rotational speed and F is the number of scraper blades.

2.4.3 **Adhesion**

Ice has the tendency to adhere to solid surfaces. General examples where this phenomenon is problematic include icing of roads, aircraft wings and power distribution networks; it is also problematic during suspension crystallization operations. The adhesive properties of ice onto solid surfaces are temperature dependent and can be ascribed to three mechanisms; interfacial chemical bonding, electromagnetic interactions (Van der Waals forces) and electrostatic interactions due to hydrogen bonding (Israelachvili, 2011).

The adhesive strength of ice on a solid surface is a function of temperature, as shown in Figure 2.6. A higher supersaturation at the cooled surface will, therefore, result in more aggressive adhesive behaviour.

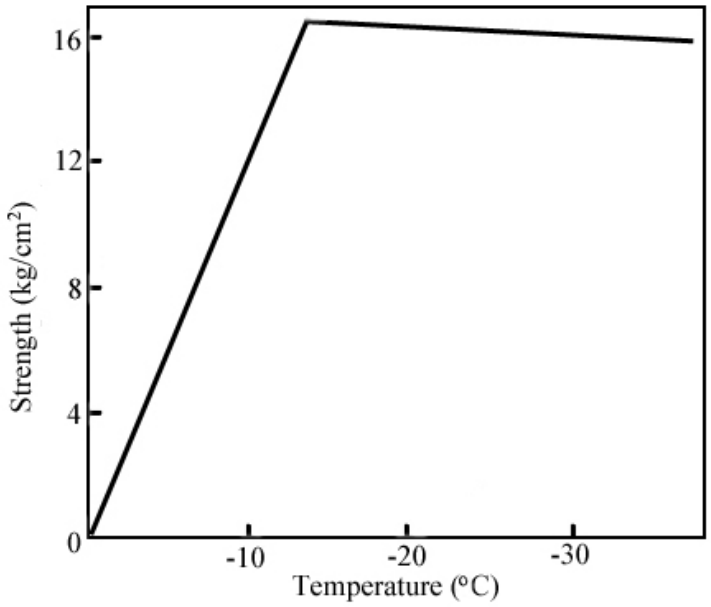

Figure 2.6: Shear strength of ice on a metal disc as a function of temperature (Petrenko, 1993)

The intramolecular bonds within water molecules are covalent bonds in which hydrogen atoms share electrons with an oxygen atom. The negatively charged oxygen atom strongly attracts the positively charged hydrogen atoms, resulting in a charge distribution within the water molecule, where the oxygen atom remains electronegative and the hydrogen atoms electropositive (Petrenko, 1993). Intermolecular hydrogen bonds form between electronegative oxygen atoms and electropositive hydrogen atoms, as depicted in Figure 2.7. Covalent bonds are much stronger than hydrogen bonds; however, each water molecule can form several hydrogen bonds resulting in a significant cumulative effect.

The hydrogen bonding within an ice lattice is ordered, giving ice a positive surface charge. The magnitude of the surface charge depends on the density of hydrogen bonding and the percentage of molecules with dipole moments oriented in a direction normal to the ice surface (Petrenko, 1993). When the ice surface is in contact with an electrolyte solution, electrostatic interaction will take place between the ions in solution and the surface of the ice. These electrostatic interactions play a major role in the adhesive behaviour of ice (Ryzhkin & Petrenko, 1997).

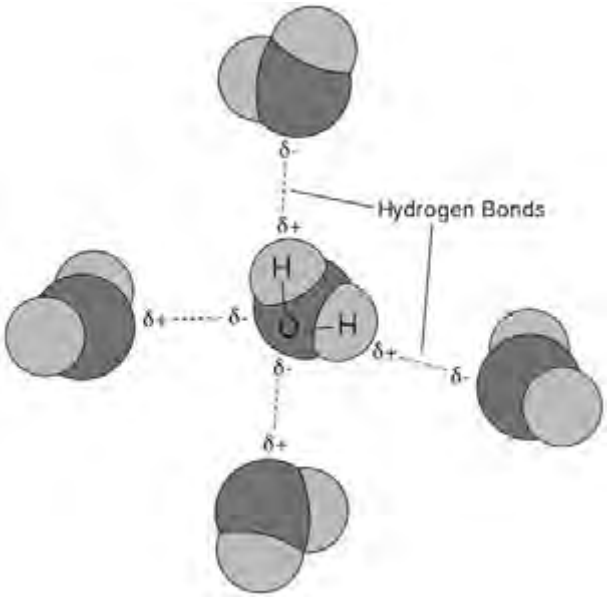

Figure 2.7: Intermolecular hydrogen bonding (Volland, 2011)

The crystallizer wall serves as a subcooled surface for adhesion of ice crystals that formed in the bulk solution. Furthermore, in scraped surface crystallizers, the mechanical scrapers are subcooled themselves, due to the continuous movement through the thermal boundary layer. Ice crystals that are scraped off the wall collide with the scraper blades and crystals which formed in the bulk solution also come into contact with the scrapers.

2.5 Heat transfer

A driving force for heat transfer is created by application of a temperature difference between process liquid and cooling medium. During cooling crystallization, supersaturation for crystallization is subsequently achieved through heat removal from the process liquid. As discussed in Section's 2.3.3.1 and 2.4, supersaturation also has a major effect on ice layer growth and the operational constraint of ice scale formation. Therefore, the rate of heat removal during crystallization processes is of interest.

2.5.1 Overall heat removal

During continuous crystallization in an indirectly cooled system, where ice and salt crystallize under eutectic conditions, the overall heat removal can be approximated by the increase in heat energy of the cooling medium, as given by Equation 2.10:

$$Q_{cm} = \dot{m} C_p \Delta T' \qquad 2.10$$

where $\dot{m}$ is the mass flow rate, C_p the specific heat capacity and $\Delta T'$ the temperature change of the cooling medium. The sensible heat of the feed as well as the heat of crystallization of both ice and salt are removed, while heat loss to the environment also occurs, as summarized by Equation 2.11:

$$Q_{cm} = Q_{feed} + Q_{ice} + Q_{salt} + Q_{loss} \tag{2.11}$$

The amount of sensible heat entering the system and heat loss to the environment can be minimized through sound design principles, rendering the rate of heat removal proportional to the rate of crystallization (Rodriguez, 2009).

2.5.2 Heat transfer resistances

In cylindrical, jacketed cooling crystallization vessels, heat transfer occurs from the bulk solution through the crystallizer wall to the cooling medium, as depicted in Figure 2.4(a). The thickness of the crystallizer wall is typically small compared to the diameter of the vessel; therefore, the expression for the overall heat transfer coefficient through a flat heat exchanger surface applies, as given by Equation 2.12 (Baehr & Stephan, 1998):

$$\frac{1}{U_o} = \frac{1}{\alpha_b} + \frac{1}{\alpha_{wall}} + \frac{1}{\alpha_{cm}} \tag{2.12}$$

where α_b, α_{wall}, and α_{cm} are the heat transfer coefficients of the bulk solution, wall and cooling medium. The overall heat transfer coefficient can be calculated using Equation 2.13:

$$U_o = \frac{Q_{cm} - Q_{loss}}{A_{ht}(T_b - T_{cm})} \tag{2.13}$$

where A_{ht} is the heat transfer area, T_b is the temperature of the bulk solution and T_{cm} is the average temperature of the cooling medium.

In general, heat transfer between a non-stationary fluid and a solid surface can be described by the dimensionless Nusselt number, where higher Nusselt numbers represent higher rates of heat transfer associated with turbulent flow conditions (Baehr & Stephan, 1998). The general relationship between the convective heat transfer coefficient and the Nusselt number is given by Equation 2.14:

$$Nu = \frac{\alpha L}{\lambda} \tag{2.14}$$

where L is the characteristic length and λ is the thermal conductivity of the fluid.

Heat transfer on the process side of a cylindrical, scraped surface heat exchanger can be described by Re-Pr-relations and penetration theory. Expressing heat transfer in terms of heat convection and fluid flow, the general form of Re-Pr-relations are used, as given by Equation 2.15 (Baehr & Stephan, 1998):

$$Nu = WRe^{b}Pr^{c} \tag{2.15}$$

where W is a constant, exponent b has a value between 0.5 and 1, and exponent c is approximately 0.3. The Reynolds and Prandtl numbers are given by Equations 2.16 and 2.17:

$$Re = \frac{\rho n L^2}{\eta} \tag{2.16}$$

$$\mathrm{Pr} = \frac{\eta C_p}{\lambda} \tag{2.17}$$

where ρ is the density of the process fluid, n is the rotational scraper speed, L is the inside diameter of the crystallizer, η is the viscosity, Cp the specific heat capacity and λ the thermal conductivity of the process fluid.

Penetration theory expresses heat transfer in terms of heat conduction and allows a description of the effect of the number of scraper blades on the heat transfer coefficient of the solution within a scraped-wall crystallizer. Penetration theory is based on the assumption that only conductive heat transfer takes place from a stationary boundary layer to the solid crystallizer wall. With each scraper pass, the boundary layer is removed; completely mixed into the bulk solution and replaced by fluid of the same thermal characteristics as those of the bulk (De Goede, 1988). A correction factor can be applied to account for non-ideal mixing. Based on penetration theory, the heat transfer coefficient in the bulk solution is given by Equation 2.18 (De Goede & De Jong, 1993):

$$\alpha_b = K_{pen}\sqrt{\frac{\lambda \rho C_p J n}{\pi}} \tag{2.18}$$

where K_{pen} is an empirical correction factor, λ is the thermal conductivity, ρ the density and C_p the specific heat capacity of the fluid, J is the number of scraper blades and n is the rotational scraper speed.

Heat transfer through the wall of the crystallization vessel is dependent on the material of construction and can be calculated using Equation 2.19:

$$\alpha_{wall} = \frac{\lambda_{wall}}{\delta_{wall}} \quad 2.19$$

where λ_{wall} is the thermal conductivity and δ_{wall} the thickness of the crystallizer wall.

Within the jacket of a cylindrical crystallization vessel, heat transfer through the cooling medium can be described by empirical models developed for flows in tubes and ducts. A correlation which has been applied successfully to cooling in tubes, under turbulent flow conditions is given by Equation 2.20 (Dittus & Boelter, 1985):

$$Nu = 0.024 Re^{0.8} Pr^{0.3} \quad 2.20$$

In the laminar regime, Nusselt numbers of 3.66 and 6 have been proposed for fully developed tube flow and flow through a rectangular duct respectively (Kakaç, Shah & Aung, 1987).

2.6 Continuous crystallization

2.6.1 Process variables

In a continuous crystallization process, the agitation rate and residence time are two important process variables which determine the distribution and consumption of supersaturation in the bulk solution as well as at the cooled surface. These variables can be manipulated to achieve the desired production rate and purity of products.

2.6.1.1 Agitation

The primary purpose of agitation in a crystallizer is the homogeneous distribution of supersaturation. Agitation improves mass and heat transfer and can inhibit the formation, or at least reduce the thickness, of a stagnant boundary layer adjacent to the cooled crystallizer wall. Vigorous agitation, however, increases the number of crystal collisions which can cause a high rate of attrition (Mullin, 2001). During EFC in a hybrid crystallizer-separator, where production and separation is achieved in the same vessel, the mixing regime must be designed to allow homogeneous supersaturation distribution without compromising gravitational separation.

For agitated vessels, relationships exist to determine the smallest size particle that will just settle to the bottom within a fixed flow regime. Equation 2.21 (Zwietering, 1958) is one such equation and allows the determination of the minimum stirrer speed to suspend particles of

size d and smaller. When the desired particle size from a crystallization process is known, such an equation can be used in the design of the mixing equipment.

$$N = S(\nu^{0.1} d^{0.2} X^{0.13} D^{-0.85} \left(g \frac{\Delta\rho}{\rho_l}\right)^{0.45}) \quad 2.21$$

In Equation 2.21, ν is the kinematic viscosity, d is the particle size, X is the fraction of solids in the system, D is the impeller diameter, g is gravitational acceleration, Δρ is the difference between the solid and liquid density, ρ_l is the liquid density and S is a dimensionless constant. S is calculated based on the diameter of the vessel and the size and shape of the impeller; Zwietering (1958) can be consulted for a large range of values. For EFC applications, the design of mixing equipment is complicated by the dual requirements for ice and salt, where suspension movement must also allow ice crystals to reach the desired size before separation takes place.

In scraped surface crystallizers, scrapers usually serve as the primary mixing device generating substantial flow and turbulence. The flow regime depends on the shape, size and number of scraper blades in relation to the volume and geometry of the crystallizer. Determination of the flow regime in a scraped crystallizer is fairly complex and general equations for its analysis are not available.

2.6.1.2 Residence time

In continuous crystallization, residence time refers to the average time that a solution or solid particle spends within a crystallizer of fixed volume. The residence time can be altered by changing the feed flow rate and has a significant influence on the size of crystals forming in suspension at low supersaturation (Chivavava, 2013). For a fixed production rate, a shorter residence time would require a higher rate of heat removal per unit volume of crystallizer due to the increased feed rate and its accompanying sensible heat.

2.6.2 **Stages in continuous crystallization**

Continuous crystallization involves a start-up stage, ideally followed by a long period of steady state operation and eventually shut-down. During start-up, a solution is cooled to slightly below its equilibrium temperature. At this point, as the solution approach the upper bound of the metastable zone, supersaturation is at a maximum and therefore, the driving force for scaling to occur is also at its highest. As nucleation occurs, supersaturation is consumed and crystal surface area is created in the bulk solution where secondary nucleation

and growth can now take place. Following the start of nucleation is an unsteady period during which the magma density adapts to its steady state value, in accordance with the rate of heat removal. Nucleation, however, is very fast in comparison to growth and the lag between the two processes results in periods of high supersaturation dominated by nucleation and periods of low supersaturation dominated by growth (Mullin, 2001). Depending on the process conditions, this stage of unsteady, periodic behaviour can be short and damped, as shown in Figure 2.8(a) or long and profound, as shown in Figure 2.8(b), where P denotes production rate, M, magma density and S, supersaturation.

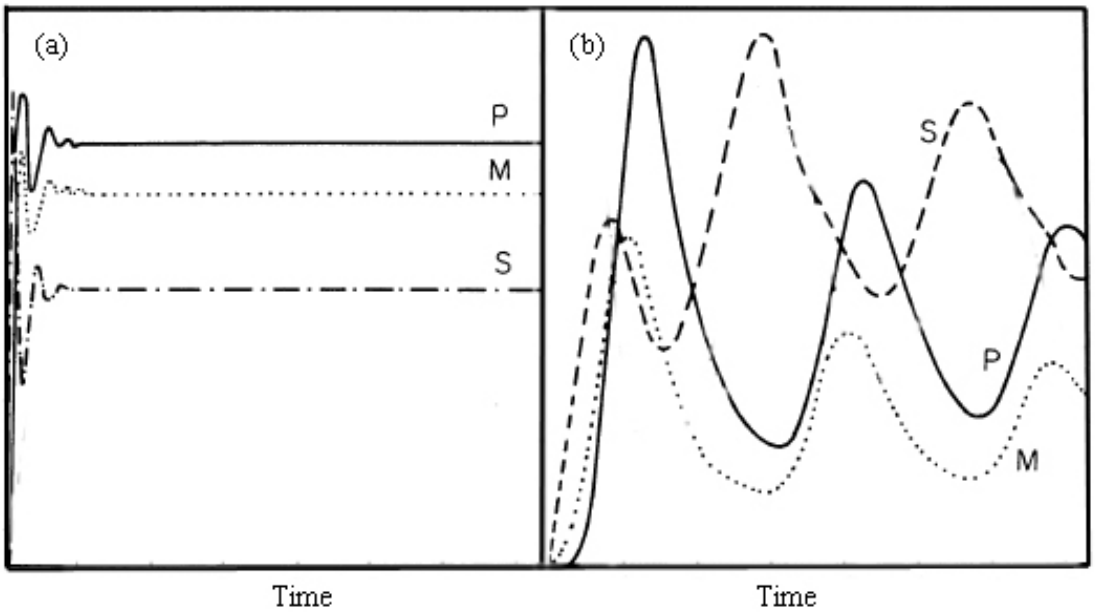

Figure 2.8: Dynamic behaviour during start-up of a continuous crystallization process (a) short and damped, (b) long and profound (Mullin, 2001)

Steady state is usually defined in terms of macroscopic variables which can be measured with ease, such as temperature in the bulk solution and production rates. When steady state is disrupted due to a step change in process conditions, similar periodic behaviour as described for the start-up period will prevail, until a new steady state is reached. Conditions which are not conducive to any steady state will eventually lead to process failure.

2.7 Magma density

The magma density, or mass of crystals per unit volume of suspension, is an operating condition dependent on the heat removal rate, residence time and solute concentration in a crystallizer. In continuous crystallization, secondary nucleation is the dominant form of

nucleation providing surface area for crystal growth. The magma density, therefore, has a major effect on crystal structure, production rate and separation efficiency of the process. The magma density also has an influence on the scaling behaviour of the system due to the surface area it provides for growth and its effect on fluid flow and the distribution of supersaturation (Mullin, 2001).

2.7.1 Factors affecting magma density

The rate of crystallization is proportional to the rate of heat removal in a crystallizer (Rodriguez, 2009). It follows logically that the magma density should show the same proportionality to the magnitude of the driving force for heat transfer, as shown in Figure 2.9:

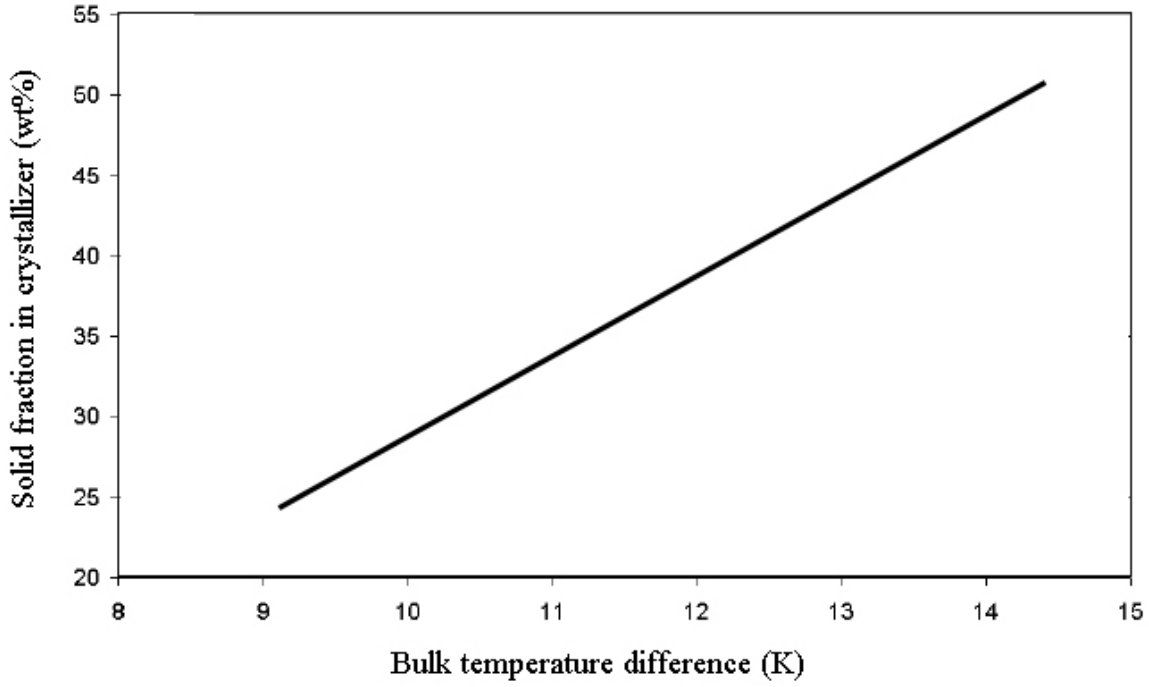

Figure 2.9: Magma density as a function of the driving force for heat transfer (Tähti, 2004)

The residence time or solids holdup time in a crystallizer represents the time allowed for a unit volume of solution to crystallize; therefore, during EFC, longer residence times are generally associated with higher magma densities. A build-up in density associated with unsteady behaviour can result from product outlet blockages, zones of no or impeded fluid flow and subcooled surfaces within the crystallizer where adhesion prevents product removal (Mullin, 2001).

2.7.2 **Measurement**

During the crystallization of ice, the accurate measurement of magma density is difficult since melting of crystals during sampling and subsequent filtration or settling operations introduces a potentially large error. For the special case of agitated vessels with homogeneous mixing and the availability of specialized equipment such as a cold room or temperature controlled filter, the magma density can be estimated by conducting a mass balance over the filter (Tähti, 2004). If a represetative sample is filtered and it is assumed that the crystals are 100 % pure and no melting occurs during filtration, the mass of solution remaining in the filter cake can be calculated according to Equation 2.22:

$$m_{RM} = \frac{x_{2,FC} m_{FC}}{x_{2,filtrate}} \tag{2.22}$$

where $x_{2,FC}$ is the mass fraction of solute in the filter cake, m_{FC} is the total mass of the filter cake and $x_{2,filtrate}$ is the mass fraction of solute in the filtrate. Again using the mass balance, the solids mass fraction in the crystallizer can then be calculated according to Equation 2.23:

$$X = \frac{m_{FC} - m_{RM}}{m_{tot}} \tag{2.23}$$

where m_{tot} is the total mass of the sample taken for filtration.

2.7.3 **Effect on scale formation**

The mechanisms involved in scale formation include adhesion, nucleation and growth. Magma density in the bulk solution affects these processes in different and often opposing ways, resulting in its complex relationship with the rate of scale formation.

A higher magma density results in a higher number of crystals coming into contact with the wall, which promotes adhesion. However, the rate of attrition is also higher because the force with which crystals hit the wall causes partial removal of other crystals and breakup of crystal layers (Söhnel et al., 1996).

The apparent viscosity of the fluid passing the wall increases with an increase in magma density. This results in a higher shear stress at the wall, which can inhibit ice layer growth. In general, suspensions with a high solids content show dilatant rheological behaviour, which means that the shear stress show an exponential increase with an increase in fluid velocity, according to Equation 2.24 (Hafaiedh, 1988):

$$\tau_s = \tau_{sy} + K\gamma_s{}^e \quad 2.24$$

where τ_{sy} is the shear stress at zero shear rate, K is a dimensionless constant, γ_s is the shear rate and e is a positive integer larger than one. The result of dilatant rheological behaviour is that a small increase in fluid flow will have a significant inhibitory effect on ice layer formation. Otherwise stated, at constant fluid velocity, a small increase in magma density will have a similar effect.

With regard to mass transfer, diffusion of solute molecules away from the growing ice front can be impeded by a high magma density, resulting in slower growth. The impedance can be due to a combination of physical obstruction and increased electrostatic interaction between negatively charged solute molecules and the electropositive ice surface.

With regard to heat transfer; fluid flow and therefore, convective heat transfer might be impeded at higher densities, promoting areas of high supersaturation at the cooled surface, which promotes scale formation. Another consideration is that high magma densities in the bulk solution provide large surface areas for crystal growth, which will reduce the supersaturation for crystal growth on the wall (Tähti, 2004).

3 Literature

Ice scale formation during freeze crystallization, and specifically EFC, of electrolyte solutions is a complex phenomenon and is influenced by many factors. These include supersaturation, the cooling configuration, the nature and concentrations of ions in solution, mixing regimes and the magma density in the crystallizer (Rodriguez et al., 2008; Vaessen, Seckler & Witkamp, 2003a). Although considerable effort has been put into design considerations to prevent scale formation, the problem has not yet been solved, nor is the complex interaction of the variables mentioned above fully understood. A short history of the development of indirectly cooled crystallizers is given below, from which it is evident that at large driving forces for heat transfer associated with high production rates, scaling is a major operational constraint. Relevant literature on the factors affecting scale formation is then discussed.

3.1 History of indirect cooling in freeze desalination

The first studies on the use of freeze crystallization as a desalination technology employed direct contact refrigeration methods using refrigerants such as butane and Freon-114 (Denton et al., 1974; Stepakoff et al., 1974). Direct contact heat exchangers, especially ones where the latent heat of vaporization of the refrigerant is utilized, are superior in their heat transfer efficiency. However, entrainment of the refrigerant in the product stream necessitates more complicated separation equipment, which adds to the cost of the process.

The United States Office of Saline Water operated a freeze desalination pilot plant between 1959 and 1968 (Ganiaris, Lambiris & Glasser, 1969). During the second half of the project, the system was fitted with an indirectly cooled pre-cooler, but the crystallizer itself was cooled by direct circulation of a butane mixture through the bulk solution. A top layer of liquid butane was maintained in the crystallizer and a central paddle-type stirrer with two blades rotated through the refrigerant, dispersing it into the bulk solution. Partial vaporization of the butane took place with vapours being removed by a compressor and the remaining liquid droplets recirculated through the solution. Using this configuration, more than 150 experimental runs were performed of which only 16 were reported as successful. During the

134 unsuccessful runs, true steady state could not be achieved with the formation and accumulation of ice on agitator blades cited as the biggest operational difficulty.

One of the earliest laboratory studies employing indirect cooling was performed in 1970, following the pilot plant work discussed above (Estrin, 1970). The crystallizer used by Estrin (1970) consisted of two concentric cylinders; the inner cylinder rotated on its axis and was cooled from the inside while the outer cylinder was stationary and cooled from the outside. During continuous operation, ice scaling on the cooled surfaces precluded many experiments. Undercooling was not accurately measured, however, it was concluded that the investigated configuration was only functional under conditions where the driving force for heat transfer was limited to a very small temperature difference between the coolant and bulk solution. During experiments where electrolyte solutions were employed as opposed to pure water, scaling was less severe. The research highlighted the ice fraction, heat transfer driving force and flow velocity as the most important variables influencing undercooling and, therefore, ice nucleation on the cooled surface. Although the contributions of ice growth and adhesion on the cooled surface were not recognized, this study was the first to give insight into the specific factors affecting scale formation and, as such, was influential in informing future designs.

A conceptual design for an indirectly cooled desalination plant was done by Johnson (1979). He used the basic concept of a shell-and-tube heat exchanger in which the aqueous slurry flows through the tubes and the latent heat of vaporization of a refrigerant is used on the shell side. Johnson (1979) recognized ice scaling as the biggest operational constraint and hence, allowed for a defrost cycle. The surface area for heat transfer was over designed, allowing 10 % of the surface to be exposed to a hot gas discharge from the primary compressor. Continuous operation was maintained by rotating the hot gas outlet and redirecting slurry flow to avoid the heated areas (Johnson, 1979).

Two decades later, a cooled disk column crystallizer (CDCC) was specifically designed for EFC, where salt and ice form under the same conditions. In the CDCC, refrigerant was circulated through disks, situated at different heights within a cylindrical vessel, as shown in Figure 3.1. The disks were mechanically scraped, to remove ice from the cooled surfaces. The feed stream was situated at middle height and crystals could move vertically through holes in the disks, to allow separation of products based on density differences (Van der Ham, 1999). The scraping mechanism was tested during EFC of several electrolyte solutions. In general, scaling did not occur at small heat transfer driving forces, however, as the driving

force was increased, a scale layer formed on the cooled surfaces (Van der Ham, Seckler & Witkamp, 2004). A second generation CDCC was later designed with improved plate, scraper and crystallizer geometry, which allowed larger driving forces without the onset of scaling (Genceli, Gärtner & Witkamp, 2005).

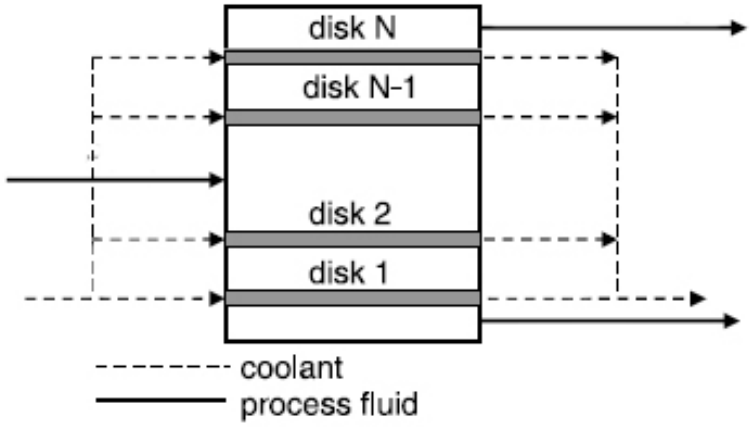

Figure 3.1: Operation of a cooled disk column crystallizer (Van der Ham et al., 2004)

Around the same time that the CDCC was developed, another design specific for EFC was introduced, namely the scraped cooled wall crystallizer (SCWC). The first generation SCWC was made of two concentric cylinders, cooled from the inside and outside, as shown in Figure 3.2. Mechanical scrapers were fitted to scrape the cooled surfaces. Gravity separation compartments were introduced above and below the cooled section, to allow separation of products. The performance of the SCWC was found to be slightly better to that of the first generation CDCC (Vaessen et al., 2003b). Improvements were made to the SCWC design by Rodriguez in 2009, which enabled the application of a higher maximum driving force for heat transfer. During EFC of binary $MgSO_4$ and HNO_3 solutions, steady state could be achieved at driving forces in excess of 9 °C, the highest driving forces successfully applied during indirectly cooled suspension crystallization. A third generation SCWC was developed in which a central stirrer was placed in the crystallization zone, to improve mixing and the distribution of supersaturation (Rodriguez & Lewis, 2013). The addition of the stirrer reduced scaling tendencies by reducing the thickness if the thermal boundary layer. This configuration was especially successful in enabling tight control over the conditions within the crystallizer, including the operational magma density and crystal size distribution (Chivavava, 2013).

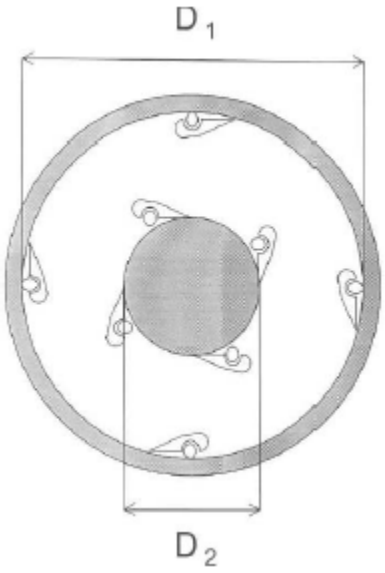

Figure 3.2: Cross section of a scraped cooled wall crystallizer (Vaessen et al., 2003b)

The most recent configuration to be evaluated in an attempt to find a solution to the still lingering problem of ice scale formation was the fluidized bed crystallizer. As mentioned in Section 2.4.2, in a fluidized bed, metal particles mechanically remove ice from the crystallizer walls during fluidization. The fluidized bed proved less effective at combatting scale formation than the SCWC. The maximum driving force that could be applied across the cooled surface without the onset of scaling was 7.5 times smaller in the fluidized bed than in the first generation SCWC (Pronk, 2006).

3.2 Factors affecting scale formation

3.2.1 Rotational scraper speed

3.2.1.1 Driving force for heat transfer

In a scraped surface crystallizer, Pronk and co-workers (2005) determined the relationship between the rotational speed of scraper blades and the maximum driving force for heat transfer that could be applied across the cooled wall, without the onset of scaling. A potassium nitrate aqueous solution was used and the scraper speed kept constant during each experiment, while increasing the driving force for heat transfer every 15 minutes by lowering the coolant temperature. Scraper speeds were varied in consecutive experiments. Contrary to what was expected, the maximum driving force decreased with an increase in scraper speed. A possible explanation for this unexpected result might be that the higher heat transfer rates achieved at higher scraper speeds allowed a build-up of magma density during the early

stages of the experiments, which caused a maldistribution of supersaturation once a higher driving force was subsequently applied. At lower scraper speeds, the magma density did not increase to the same extent and radial flow might have been sufficient to prevent scaling upon application of higher driving forces. Although Pronk and co-worker's (2005) study provides insight into the relationship between scraper speed and heat transfer driving force, it does not give information on the scaling behaviour during steady or pseudo steady state, as the driving force was varied every 15 minutes. Lakhdar and co-workers (2005) investigated the same relationship during experimental work on aqueous sucrose and water-ethanol solutions, at scraper speeds in excess of 800 rpm. Lakhdar and co-workers (2005) found a contradictory relationship where an increase in rotational speed of scrapers resulted in a decrease in scaling tendencies, as would be expected.

3.2.1.2 Heat transfer coefficient

Lakhdar and co-workers (2005) found a correlation for the heat transfer coefficient as a function of scraper speed during crystallization; however, it was specific to the type of solution and scraper used. The heat transfer coefficient increased with an increase in scraper speed. Vaessen and co-workers (2003a) measured the specific heat flux prior to nucleation as a function of scraper speed. As expected, the heat flux increased with an increase in scraper speed; however, during EFC of a ternary KNO_3-HNO_3 solution, it was observed that the heat flux decreased, as the scraper speed was increased from 34 rpm to 65 rpm. The decrease in heat flux was attributed to a higher operational magma density at the faster scraper speed, which limited convective heat transfer by impeding radial fluid flow. From the studies of Lakhdar and co-workers (2005) and Vaessen and co-workers (2003a), it is clear that during crystallization, the relationship between scraper speed and heat transfer coefficient is a complex function of the mixing and cooling configuration, nature of the solution and magma density within the crystallizer.

3.2.1.3 Thermal boundary layer

In general, the action of scraping removes the thermal boundary layer in addition to mechanically removing ice crystals from the solid surface. During crystallization of several electrolyte solutions in a scraped surface crystallizer, Vaessen, Himawan and Witkamp (2002) fitted scraper blades with soft silicone tips, to determine whether mere removal of the thermal boundary layer was sufficient to prevent ice scaling. At high driving forces for heat transfer, scaling rapidly occurred when silicone tips were used, and it was concluded that

mechanical removal of ice from the surface was indeed necessary for scale prevention. Higher normal forces exerted by the scrapers also improved scale prevention (Vaessen et al., 2002), suggesting that improved mechanical ice removal deterred scaling. Contrary to what Vaessen and co-workers (2002) found, Lakhdar and co-workers (2005) reported that positioning the scrapers 1 mm above the cooled surface was effective in scale prevention, but positioning the scrapers 3 mm above the cooled surface was ineffective. These contradictory findings lead one to suspect that scaling behaviour is not only dependent on the efficiency of boundary layer removal, but on the total flow regime in the crystallizer.

3.2.2 **Solute type**

The nature of the ionic species in solution affects scaling behaviour by affecting the adhesive forces between ice and solid surfaces. As discussed in Section 2.4.3, Ryzhkin and Petrenko (1997) found that adhesive forces are governed by electrostatic interactions, related to the surface charges on ice. These electrostatic interactions are specific to the nature of ions in solution.

A systematic investigation into scale formation during continuous crystallization of electrolyte solutions was done by Vaessen and co-workers (2002). In their experiments, an initial scraper speed of 100 rpm was used and this was lowered in stages, at 10 minute intervals, until scaling was observed. The time between scraper passes, at the point at which scaling was observed, was recorded and defined as the critical time for the onset of scaling. A shorter critical time, therefore, represents more aggressive scaling behaviour. The scaling behaviour of binary KNO_3, HNO_3, $CaCl_2$, $MgSO_4$ and H_2SO_4 solutions were investigated. The critical time was found to be unique to dissolved ionic species, at constant supersaturation (Vaessen et al., 2002). The results, in order of increasing critical times are as follows: $CaCl_2$ < KNO_3 < $MgSO_4$ < H_2SO_4 < HNO_3. Vaessen and co-workers (2002) postulated that the interaction of the solute molecules with the ice surface reduce the positive surface charge and by doing so, reduce the adhesive force of ice onto the cooled crystallizer surface. This postulation is reasonable, since the interaction could cause a decrease in the density of hydrogen bonding between water molecules in the ice lattice. In addition to differences in adhesive strength, unique critical times were attributed to differences in the growth rates of ice following heterogeneous nucleation.

Vaessen and co-worker's (2002) results clearly show that scaling behaviour is dependent on the nature of dissolved ionic species. However, it does not provide information on this

relationship during steady state operation. A change in process conditions, such as a change in scraper speed, has an effect on the rate of heat transfer, which in turn affects the magma density and distribution of supersaturation in the crystallizer. It cannot be assumed that the response time of the process is less than 10 minutes, nor can it be assumed that the long-time response is either similar to the short-time response or insignificant in itself. Literature on the effect of the nature of ions in solution on scaling behaviour over extended periods of time, and approaching steady state, could not be found.

3.2.3 **Solute concentration**

Since the growth rate of ice is limited by either the heat transfer rate, mass transfer rate or surface integration kinetics, the concentration of ions in solution influence scaling behaviour because it affects the rate of mass transfer (Huige, 1972). In the experiments discussed in Section 3.2.2, Vaessen and co-workers (2002) also varied the concentrations of the five electrolyte solutions and found that an increase in solute concentration resulted in an increase in critical time for all five solutions, at constant supersaturation. Pronk (2006) modelled the contributions of heat transfer, mass transfer and surface integration to the total resistance to ice layer growth for NaCl solutions of varying concentration and found that the growth rate of ice is primarily mass transfer controlled at higher solute concentrations (Figure 3.3). After nucleation, the number of solute particles that have to diffuse away from the growing ice front is higher at higher concentrations, and growth rates show a linear decline with an increase in solute concentration (Pronk, 2006).

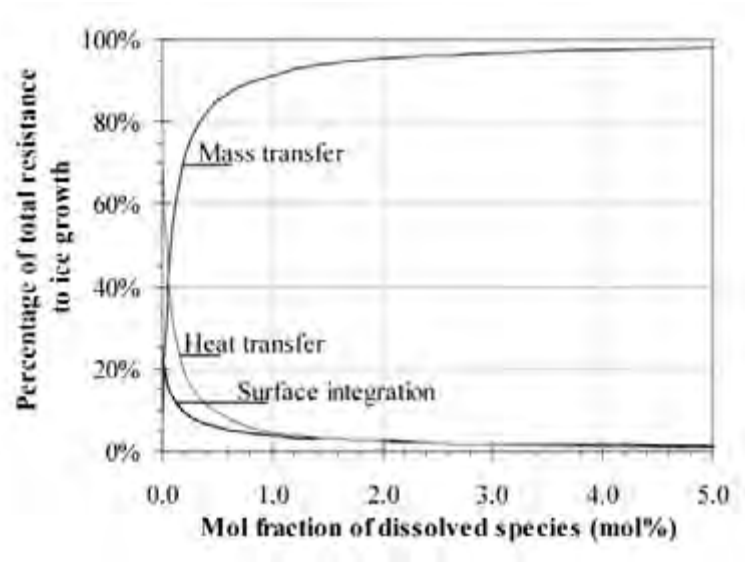

Figure 3.3: Contributions to the total resistance to ice layer growth for binary NaCl solutions (Pronk, 2006)

An interesting observation was made by Pronk and co-workers (2005) during a study of the concentration dependence of ice scaling. The maximum temperature difference that could be applied across the cooled surface, during continuous crystallization of dilute KNO_3 solutions, was determined. The maximum temperature difference increased linearly with concentration, up to the eutectic point, at which it decreased. Pronk and co-workers (2005) postulated that, because of the simultaneous crystallization of solute and ice at the eutectic point, the mass transfer limitation is not as profound due to the contributing factors of both solute crystallization and solute diffusion.

3.2.4 **Magma density**

3.2.4.1 Continuous crystallization

The influence of magma density on scaling behaviour in continuous, indirectly cooled systems has not been studied systematically, but insight can be gained by looking at several studies in which magma density was reported. In the studies discussed below, magma density during continuous operation varied from very low, to more than 35 %. Densities were estimated based on visual observations or measurement of production rates, with the exception of Genceli and co-workers (2005) who used a more accurate technique which involved sampling of the CDCC at different heights.

Estrin (1970) operated a laboratory sized crystallizer in which the magma density was sufficiently low to allow photographic analysis of the crystal size distribution. The work

aimed to investigate the secondary nucleation rate of ice in continuous crystallization; however, problems with scale formation were so severe that no conclusive results could be reported. The option of increasing the magma density was not considered as this would have rendered photographic analyses inaccurate.

Vaessen and co-workers (2003a) worked with magma densities ranging from 6 % to 10 %. The inverted relationship between scraper speed and heat flux, discussed in Section 3.2.1.2, was attributed to an increase in magma density, even within this small range. At the higher magma density of 10 %, visual observations indicated that fluid flow in the radial direction was impeded. Although no ice could be seen on the crystallizer wall, it was postulated that the reduction in heat flux was due to the formation of a transparent scale layer. The pilot scale work done by the US Office of Saline Water was in the intermediate density range, from 11 % to 14 %, during both the successful and unsuccessful experiments. Ice was reported to form on impeller blades when the driving force for heat transfer exceeded 2 °C. It can be deduced that the magma density within this range did not prevent the effective distribution of refrigerant within the bulk solution and as such was not the dominant factor determining scaling behaviour. No experiments were done at densities below or above this range (Ganiaris et al., 1969). Using the second generation CDCC, Genceli and co-workers (2005) did experimental work with a binary eutectic aqueous magnesium sulphate solution. At solids densities between 14 wt% and 21 wt%, no scaling was observed even at temperature differences in excess of 6 °C. In the second generation SCWC, operational magma densities between 20 % and 36 % did not result in any scaling problems, however, when the density increased above 40 %, rapid scale formation occurred (Rodriquez, 2009).

3.2.4.2 Batch crystallization

Batch crystallization provides a platform where the effect of magma density on scaling behaviour can be studied, since the magma density can be calculated with accuracy by virtue of the heat removal rate. Following the difficulties experienced in continuous crystallization by Estrin (1970), he proceeded to investigate the secondary nucleation rates of ice in batch crystallization. Photographic analysis was made possible by circulating a small portion of the slurry through an external cell at specific time intervals. It was found that a much larger range of temperature driving forces could be investigated without scale formation. The authors attributed the decrease in scaling tendencies to the higher magma density during batch operation. Qin and co-workers (2003) measured the heat transfer and rotational scraper

torque during batch crystallization of a 10 wt% sucrose solution. The rotational torque showed a gradual increase from nucleation until the scrapers reached the maximum torque that the scraper motor could supply. The maximum torque was reached consistently at a magma density of approximately 60 %, an observation which was explained by an increase in the apparent viscosity of the fluid and, therefore, a higher resistance to scraper action. The calculated Reynolds numbers indicated that the flow regime changed from turbulent to laminar, just before the maximum torque was reached. Ice adhesion to the cooled surface and its subsequent removal was deemed to make only a minor contribution to the rotational torque. Heat transfer showed a step increase during nucleation, after which it remained stable until the maximum torque was reached (Qin et al., 2003).

3.2.4.3 Summary: Magma density ranges

From the studies discussed above; it is clear that scale formation is more prevalent when operating at either very low or very high magma densities. At low densities, very little ice is available in the bulk solution for secondary nucleation and growth, therefore, the preferred pathway for supersaturation consumption seems to be through heterogeneous nucleation and growth on the cooled wall. At the very high end of densities, fluid viscosity becomes very high, resulting in poor radial mixing and a very high supersaturation at the cooled surface, promoting scale formation. In the intermediate density range, some problems were reported, but many more successful operations were possible (Genceli et al., 2005; Vaessen et al., 2003a; Ganiaris et al., 1969). It can be deduced that an intermediate range of densities exist, where the distribution of supersaturation is not compromised, while the available ice surface area is enough that the majority of supersaturation is consumed by nucleation and growth in suspension. Scaling within this region is less severe and magma density is not the dominant factor determining scaling behaviour.

3.3 Scale formation during the different stages of continuous operation

During a continuous crystallization process, the start-up stage has the most favourable conditions for the formation of a scale layer, as discussed in Section 2.6. In order to avoid scale formation during this period of maximum supersaturation, Tähti (2004) kept the driving force for heat transfer small during start-up and slowly increased it after nucleation, giving the magma density time to develop in relation to the increased driving force. This method was effective in preventing scale formation; however, it prolonged the start-up process as the cooling rate was low. In order to maintain a fast rate of cooling, Van der Ham and co-workers

(2004) combatted this peak in supersaturation by starting with the desired low coolant temperature, but increasing it as soon as crystals were seen on the cooled surface. The coolant temperature was lowered again soon after nucleation and maintained for the duration of the experiment. Both methods proved effective at preventing scale formation during the start-up stage.

Van der Ham and co-workers (2004) reported unexpected scaling behaviour after several hours of operation. During EFC of a copper sulphate solution in the CDCC, scaling was observed after more than six residence times of seemingly stable operation had passed. No systematic investigation into the time between nucleation and scale formation was done, but this time interval did vary significantly between experiments in which the residence time and coolant temperature differed. Van der Ham and co-workers (2004) attributed the variance in the magnitude of this time interval to the stochastic nature of primary nucleation. The same behaviour was seen in the SCWC, where scaling was observed after several hours of operation. It was postulated that ice grows slowly within the surface roughness of the wall and only after several hours has grown to such an extent that steady state is disrupted on a macroscopic scale (Vaessen et al., 2003b).

4 Context and motivation

4.1 Gap analysis

Ice scale formation is an operational constraint which is encountered during the application of large driving forces for heat transfer, associated with high production rates, as discussed in Section 3. The formation of an ice layer on cooled heat exchanger surfaces reduces the heat removal rate from the crystallizer and poses a risk to process equipment; therefore, the need for systematic investigation of the ice scaling phenomenon exists.

An ice scale layer has been observed to form after several residence times of seemingly steady state operation (Van der Ham et al., 2004; Vaessen et al., 2003b). However, relevant systematic investigations only report on scale formation within very short time frames, between 10 and 15 minutes after reaching the conditions under study (Pronk et al., 2005; Vaessen et al., 2002). Further still, conflicting findings on the effect of mechanical scraping on ice scaling behaviour are reported (Lakhdar et al., 2005; Vaessen et al., 2002). Investigating ice scaling behaviour under different operating conditions within longer time frames would be beneficial to the development of indirectly cooled continuous eutectic crystallizers.

An analysis of previous research has shown that the mixing regime in the crystallizer has a major effect on ice scaling behaviour (Lakhdar et al., 2005; Vaessen et al., 2002). The mixing regime is determined by the movement of scrapers as well as any secondary mixing device, such as a central stirrer. In order to investigate individual contributions to the prevention of ice scale formation, operating regimes are distinguished, as shown in Figure 4.1. The scope of the current project is to investigate scaling behaviour in a crystallizer which is scraped, but not stirred. In this regime, the thermal boundary layer is allowed to form in between scraper passes, as graphically illustrated in Figure 2.5, and the frequency of its removal is known by virtue of the scraper speed. Therefore, by operating in this regime, the effect of thermal boundary layer removal can be investigated, without partial removal happening between scraper passes. The current research was aimed at the lower end of scraper speeds, as indicated by the black box in Figure 4.1. Scraping is energy intensive and low scraper speeds are, therefore, of industrial interest.

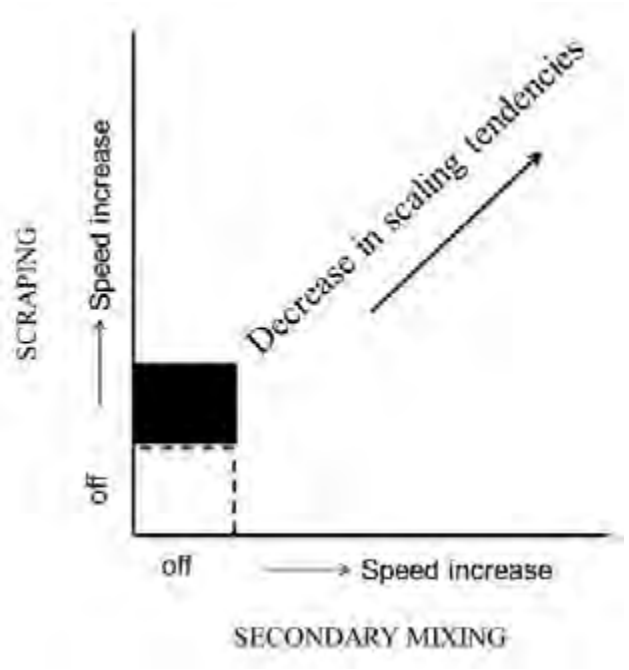

Figure 4.1: Operating regimes within an indirectly cooled crystallizer

Industrial brine streams typically contain many solute types, in varying quantities. Sodium sulphate is the primary salt in the wastewater stream from many South African mining operations, and smaller quantities of calcium sulphate, magnesium sulphate, sodium chloride and other ions are present (Gunther & Naidu, 2008). Investigation into the scaling behaviour of impure eutectic solutions is lacking in literature. The scope of this project includes investigation into the effect of several inorganic impurities within a binary eutectic solution, on scaling behaviour.

4.2 Hypotheses

A larger driving force for heat transfer result in a lower wall temperature and, therefore, a larger undercooling in the vicinity of the cooled wall. A larger driving force for heat transfer further increases the rate of crystallization by increasing the rate of heat transfer. **It is, therefore, hypothesized that an increase in the driving force for heat transfer will result in a decrease in the time taken for scale layer formation.** Scrapers remove the thermal boundary layer and distribute supersaturation and magma throughout the bulk solution. **It is, therefore, hypothesized that an increase in rotational scraper speed will increase the time between nucleation and the formation of an ice scale layer.**

The nature of the ions in solution affects the adhesive behaviour of ice on solid surfaces through electrostatic interactions. **It is, therefore, hypothesized that the presence of**

inorganic impurities in a binary eutectic solution will increase the time between nucleation and scale layer formation, and that the magnitude of the increase will be unique to dissolved ionic species. The mass transfer of solute ions away from the growing ice front is one of the contributing factors limiting the rate of ice layer growth. **It is, therefore, hypothesized that an increase in impurity concentration will result in an increase in the time between nucleation and ice layer formation on the cooled surface.**

4.3 Key questions

1. What is the effect of the driving force for heat transfer on the time taken for the onset of scaling?
2. What is the effect of scraper speed on the time taken for the onset of scaling?
3. How does the presence of inorganic impurities in a binary eutectic system affect the time taken for the onset of scaling?
4. How does the concentration of impurities in a binary eutectic system affect the time taken for the onset of scaling?

4.4 Objectives

The overarching objective of the research reported here, was to investigate some of the factors which influence scaling behaviour under eutectic conditions, in order to inform future design and operation of indirectly cooled, continuous crystallization systems. The specific objectives were as follows:

1. To investigate the effect of the driving force for heat transfer on ice scaling behaviour.
2. To determine the effect of mechanical scraping of cooled crystallizer walls on ice scale formation.
3. To determine the effect of the presence of several types of inorganic impurities on the scaling behaviour of a binary eutectic solution.
4. To investigate the effect of the concentration of selected inorganic impurities in a binary eutectic system on scaling behaviour.

5 Methodology

The methodology described in this section was used to achieve the objectives stated in Section 4.4. The experimental design is explained followed by detail descriptions of the equipment, measurement techniques and procedures applied.

5.1 Experimental design

A solution containing 4 wt% analytical grade Na_2SO_4 and 96 wt% deionised water was prepared. Experiments were conducted using an indirectly cooled, continuous eutectic crystallizer, with a capacity of two litres, as detailed in Section 5.2.1.

5.1.1 Operating conditions

Investigations into the effect of the driving force for heat transfer on the onset time for scaling were aimed at the high end of the driving force spectrum as large driving forces are associated with high production rates, but limited by operational difficulties due to ice scale formation. The range of driving forces investigated included 8.6 °C, 13.4 °C and 15.8 °C. The upper limit was determined by the maximum driving force that could be achieved by the thermostatic unit before nucleation started in the crystallizer. The lower limit was just below the maximum driving force at which successful operation was reported in relevant literature (Rodriguez, 2009).

Scraper action is energy intensive; as such, scraper speeds at the lower end of the scraper speed spectrum is of interest for industrial application. Rotational scraper speeds were varied between 2.1 rpm, 6.4 rpm and 10.7 rpm. The lowest speed attainable by the scraper motor fixed the lower limit of rotational speed investigated. The upper limit of 10.7 rpm can still be considered a relatively low scraper speed.

5.1.2 Composition of wastewater system

Simultaneous crystallization of ice and sodium sulphate decahydrate ($Na_2SO_4 \cdot 10H_2O$) occurs at a concentration of approximately 4 wt% and a temperature of approximately -1.1 °C, from the binary Na_2SO_4-H_2O system, as shown in Figure 2.1. The eutectic Na_2SO_4-H_2O system was chosen as the primary system for this investigation based on its industrial relevance.

Sulphide minerals are commonly found in South African ore bodies, with pyrite (FeS_2) being the most abundant heavy-mineral throughout the Witwatersrand gold deposits. The Merensky reef (Pt) comprise between 3 % and 10 % base metal sulphides and the Waterberg Coalfield also contain pyrite in large quantities (Coetzee, 1976). It is, therefore, not surprising that Na_2SO_4 is one of the major constituents in wastewater from South African mining operations.

Other inorganic salts, such as $CaSO_4$, $MgSO_4$ and NaCl are found in more dilute concentrations in mining wastewaters (Gunther & Naidu, 2008). At constant heat transfer driving force and scraper speed, the effect of small quantities of these salts as impurities in the eutectic Na_2SO_4-H_2O system was investigated. Calcium sulphate was added in concentrations of 0.1 wt% and 0.2 wt%, limited by its low solubility in water. Magnesium sulphate additions of 1 wt% and 3 wt% were investigated, with investigation of sodium chloride additions of 0.5 wt% and 1 wt%. These concentrations are at the lower end of the spectrum found in mining wastewater.

5.2 Experimental setup

5.2.1 Equipment

The experimental setup used throughout this study is shown in Figure 5.1. The primary crystallization apparatus was a cylindrical vessel, made of glass to allow visual observation of crystallization. The apparatus served as a hybrid crystallizer-separator, and consisted of a two litre jacketed crystallization zone (CZ), a lower separation zone (LSZ) and an upper separation zone (USZ). A Thermo Scientific 150 thermostatic unit (HE 1) was used to remove heat from the CZ by circulation of Kryo 51 coolant through the jacket. The inner wall of the CZ was scraped using scrapers made of high density polyethylene (HDPE), powered by a variable speed Bonfiglioli motor (M). Sensible heat was removed from the feed stream by a pre-cooler system consisting of two jacketed vessels (PC 1 and PC 2), each with a capacity of one litre. The pre-coolers were cooled through circulation of Kryo 51 coolant supplied by a Grant 150 thermostatic unit (HE 2). To ensure a feed stream of homogeneous concentration and temperature, the pre-coolers were equipped with overhead variable speed IKA stirrers (S1 and S2).

The ice and salt product slurries from the crystallizer were captured in a melting vessel (MV) positioned on a magnetic hot plate (HP). Mixing in the MV was achieved with a magnetic stirrer, while crystals were re-dissolved through heating. Peristaltic Watson Marlow pumps

were employed to pump the feed solution from PC 1 to PC 2 (P1), from PC 2 to the CZ (P2), salt product slurry to the MV (P3) and the re-dissolved solution from the MV to a container for disposal (P4). Pipework shown in Figure 5.1 consisted of silicone tubing, insulated with neoprene rubber. Pre-cooler vessels were also insulated, to minimise heat loss.

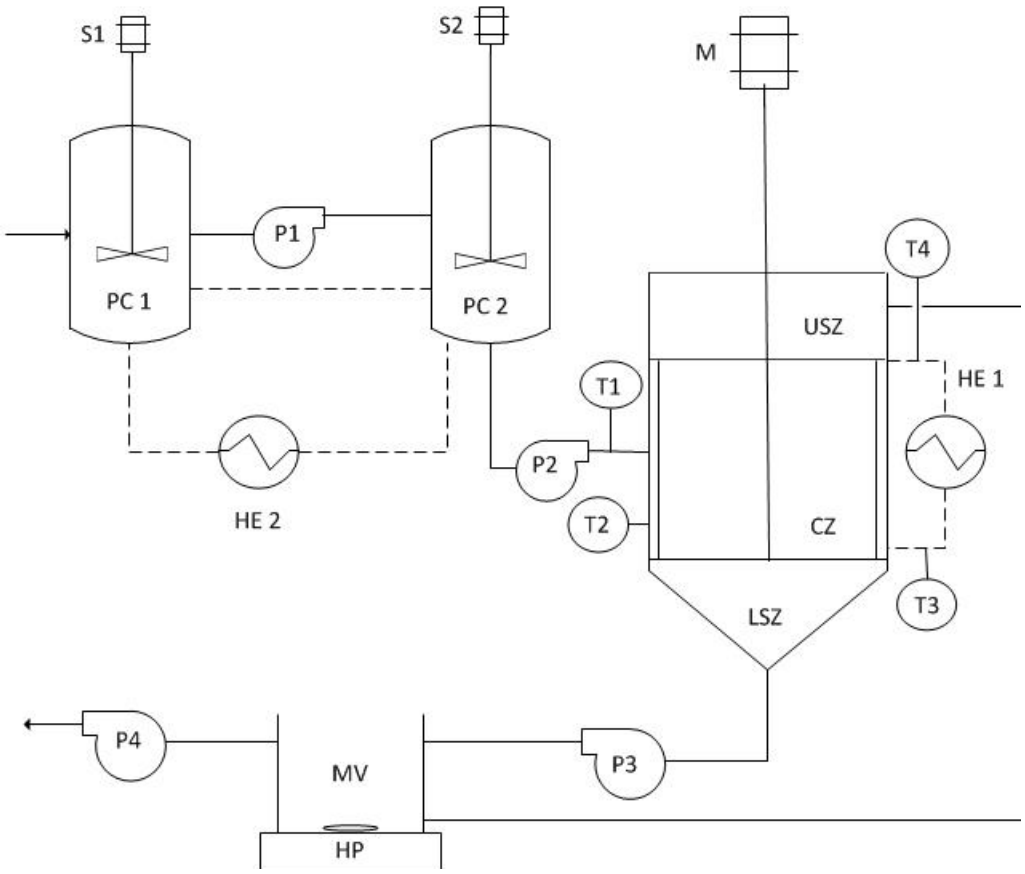

Figure 5.1: Experimental setup

The current research involved the application of very large temperature differences between the bulk solution in the CZ and the coolant flowing through the jacket, as discussed in Section 5.1.1. This also implied a large potential for heat loss from the coolant to the environment, which was at ambient temperature. As such, the crystallization vessel was well insulated with a layer of heavy duty foil between two layers of neoprene rubber. During operation, the CZ did not feel cold to the touch, indicating minimal heat loss. Small holes of approximately 2x2 cm were cut in the insulation in each of the three zones (CZ, LSZ, USZ), to allow visual observations. Holes were covered up when not in use. The HDPE scrapers were fixed to a four-armed metal frame, connected to the central shaft. Steel springs, coated with rust proof metal paint, were employed to maintain the normal force of the scrapers on the crystallizer wall.

The ice removal mechanism at the top of the USZ consisted of an outlet spout, which allowed overflow of the ice slurry, assisted by a cone and flipper fixed to the central shaft. The plastic cone was fixed at the level of the spout, serving the purpose of combatting ice accumulation which tended to occur at the shaft due to centrifugal fluid flow caused by the rotational movement of the scrapers. The plastic flipper, fixed to the cone, mechanically pushed ice through the spout at every rotation. Salt removal from the LSZ was achieved with a peristaltic Watson Marlow pump as the relatively small size of the salt crystals did not cause blockage of silicone tubing.

5.2.2 **Measurements**

The temperature of the feed solution (T1), bulk liquid (T2), coolant inlet (T3) and coolant outlet (T4) were measured with platinum resistance thermometers (Pt 100), with an accuracy of ±0.01 °C. The thermometers were connected to an F252 AC precision bridge and 16-multichannel SB 500 switchbox. Online data recording was made possible through ASL ULog V6 software.

It was possible to place probes T1, T3 and T4 at the exact locations where the measurements were preferred, as shown in Figure 5.1. Therefore, for the purpose of analysis, the accuracy of these measurements was within the accuracy of the instrumentation. However, due to the rotational movement of the scrapers, probe T2 had to be placed in the uppermost part of the LSZ. The temperature in the LSZ was slightly higher than the temperature in the CZ because the heat of crystallization released from consumption of any residual supersaturation was not removed, causing the temperature to rise. Visual observation of both ice and salt crystallization confirmed operation at the eutectic point of the Na_2SO_4-H_2O system. Based on the known eutectic temperature of -1.1 °C (Thomsen, 1997), the inaccuracy due to the location of the probe was estimated to remain approximately constant, in the order of 0.5 °C. This was deemed acceptable because of the small variation observed in the magnitude of the inaccuracy as well as the rapid rise in temperature combined with visual observations indicating the onset of scaling. All visual observations were made through 2x2 cm windows cut in the insulation material. A fibre optic connected to a white light source was used for lighting.

5.3 Experimental procedure

The continuous 2 litre EFC plant, as described in Section 5.2.1, was used for all experiments. The general experimental procedure is given in this section, with variations on the general procedure discussed under the respective headings, below. The order of experimental runs was randomized and all experiments were done in triplicate, to establish repeatability.

An aqueous solution containing 4 wt% Na_2SO_4 was made and fed to PC 1 and PC 2, where continuous stirring ensured a homogeneous concentration and temperature of the feed solution. The crystallizer was filled and continuous operation started by switching on the pumps; with the melting vessel operated at a liquid level of approximately 500 ml. Scrapers were started at the desired speed which then remained constant for the duration of an experimental run. The residence time within the CZ was kept constant at 10 minutes throughout the experimental work; this was done through control of the feed flow rate.

The temperatures of the coolant from both the Grant 150 and Thermo Scientific 150, were lowered step-wise in order to reach the desired coolant, feed and bulk solution temperatures before nucleation took place in the CZ. Once the temperature in PC 2 reached approximately -1.0 °C, it was kept constant to prevent nucleation in the pre-cooler. Some heat loss occurred between PC 2 and the CZ, mainly due to the unavoidable pumping requirement (P2) between the vessels, which resulted in a feed temperature of approximately -0.5 °C. By keeping the sensible heat of the feed solution to a minimum, heat removal in the CZ constituted primarily the removal of heat of crystallization. The benefit of this was twofold; firstly, any possible effect of sensible heat removal in the CZ on scaling behaviour was eliminated and secondly, production rates of all products per unit surface area available for heat transfer was at a maximum. It is, therefore, an operational strategy which has relevance for industrial application.

The bulk solution in the CZ was cooled down until the upper limit of the metastable zone was reached, at which point nucleation took place. All operational parameters were kept constant during crystallization, until scaling was observed. To prevent damage to the mechanical equipment and glass vessel, the system was shut-down once scaling was observed.

5.3.1 Driving force for heat transfer

Operating conditions for investigations done on the effect of the driving force for heat transfer on the onset time for scaling is shown in Table 5-1. The driving force was varied by

adjustment of the coolant inlet temperature. During each experimental run, the driving force was kept constant; it was then varied in consecutive experiments.

Table 5-1: Operating conditions for heat transfer driving force investigations

Solute	Scraper speed (rpm)	Average coolant temperature (°C)	Heat transfer driving force (°C)
4 wt% Na_2SO_4	10.7	-9.7	8.6
4 wt% Na_2SO_4	10.7	-14.5	13.4
4 wt% Na_2SO_4	10.7	-16.9	15.8

Overall heat transfer rates were calculated using Equation 2.6, with the properties of the cooling medium, Kryo 51, as given in Table 5-2 (Lauda, 2015):

Table 5-2: Heat transfer liquid data, Kryo 51

Operating temperature (°C)	Specific heat capacity (J/kg°C)	Density (kg/m^3)
-10	1570	954
-15	1560	958
-18	1560	960

5.3.2 Scraper speed

Operating conditions for investigations done on the effect of scraper speed on the onset time for scaling is shown in Table 5-3. The effect of scraper speed was investigated across the range of heat transfer driving forces. Scraper speed was kept constant during each experimental run, and varied in consecutive experiments.

Table 5-3: Operating conditions for scraper speed investigations

Solute	Heat transfer driving force (°C)	Scraper speed (rpm)	Time between scraper passes (s)
4 wt% Na_2SO_4	8.6	2.14	7.0
4 wt% Na_2SO_4	8.6	6.42	2.3
4 wt% Na_2SO_4	8.6	10.70	1.4
4 wt% Na_2SO_4	13.4	2.14	7.0
4 wt% Na_2SO_4	13.4	6.42	2.3
4 wt% Na_2SO_4	13.4	10.70	1.4
4 wt% Na_2SO_4	15.8	2.14	7.0
4 wt% Na_2SO_4	15.8	6.42	2.3
4 wt% Na_2SO_4	15.8	10.70	1.4

5.3.3 Solute type and concentration

Table 5-4 lists the types and concentrations of impurities added to the eutectic Na_2SO_4-H_2O system during investigation of the effect of electrolyte impurities on the onset time for ice scaling. A single impurity type at fixed concentration was added to the eutectic Na_2SO_4-H_2O system in individual experiments. Impurity types and concentrations were varied in consecutive experiments. Solute types and concentrations were chosen within the range found in South African mining effluents (Gunther & Naidu, 2008), however, it is acknowledged that comparison between solute types at equal molal concentration would have enabled a better understanding of the possible differences in scaling behaviour between different solute types.

Table 5-4: Impurity content for solute type and concentration investigations

Impurity	Concentration (wt%)	Molality (mol/kg)
Zero	-	-
$CaSO_4$	0.1	0.007
$CaSO_4$	0.2	0.015
NaCl	0.5	0.087
NaCl	1.0	0.174
$MgSO_4$	1.0	0.084
$MgSO_4$	3.0	0.258

To determine the effect of impurities listed in Table 5-4 on the freezing point and pH of the eutectic Na_2SO_4-H_2O system, thermodynamic modelling was done using OLI Studio 9.2 (2015). The Mixed Solvent Electrolyte (MSE) model, employing Helgeson Direct equations of state, was used with a calculation accuracy of 0.01 °C. The accuracy is similar to that of the temperature probes used in the experimental work.

6 Results and discussion

The results from the experimental work on ice scale formation, as described in Section 5, are reported and discussed below. Several general trends were observed during the majority of the experimental work; these are discussed first. Details of the experimental results at varying driving forces for heat transfer, scraper speeds, solute types and concentrations subsequently follow, including variations on the general trends.

6.1 General scaling behaviour

6.1.1 Temperature variation with time

The temperature variation with time, during a single experimental run, is shown in Figure 6.1 for crystallization from a Na_2SO_4 aqueous solution of eutectic composition. The driving force for heat transfer was 8.6 °C and scraper speed 10.7 rpm, which is the equivalent of 1.4 seconds between scraper passes. Appendix A can be consulted for examples of the temperature variation with time at different heat transfer driving forces and scraper speeds.

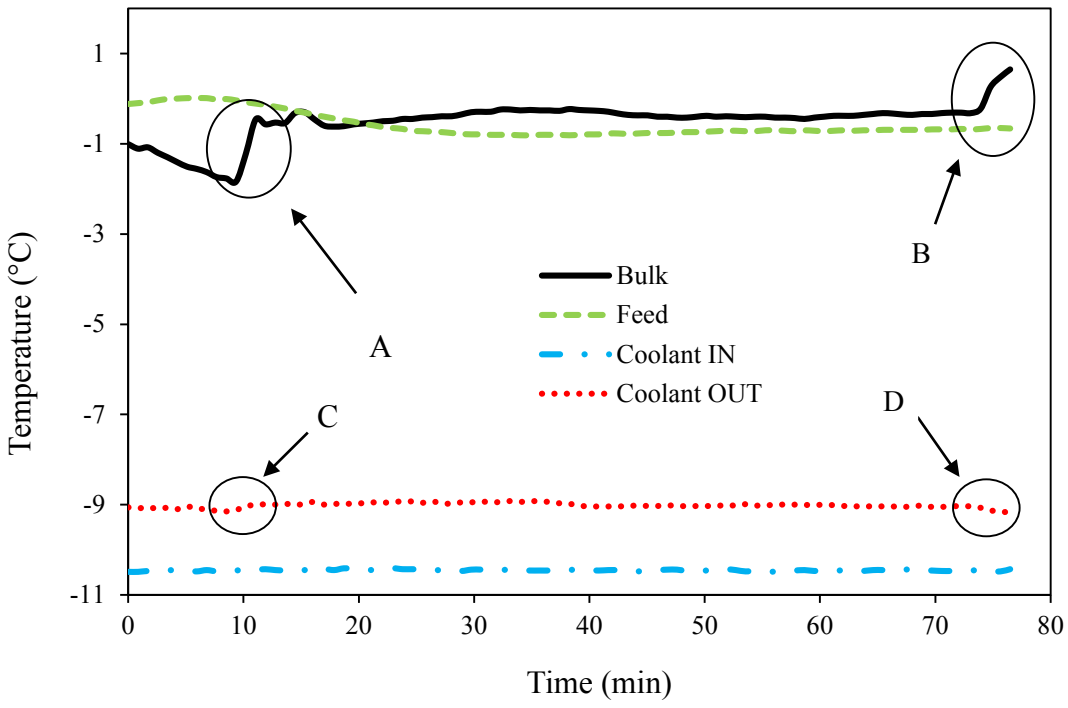

Figure 6.1: Scale formation during EFC of a binary Na_2SO_4-H_2O solution

From Figure 6.1 it can be seen that the bulk solution temperature decreased until point A, where a steep rise was observed, followed by a period of approximately constant temperature until another steep rise at point B. The outlet temperature of the coolant increased slightly at point C, which coincides with point A, and decreased slightly at point D, which coincides with point B. The coolant outlet temperature remained at a value between that of the coolant inlet and bulk solution throughout the experimental run. The inlet temperature of the coolant was kept constant at a value well below that of the bulk solution temperature, while the feed solution temperature was maintained within 0.5 °C of the eutectic crystallization temperature of the Na_2SO_4-H_2O system.

Heat removed from the bulk solution was absorbed by the coolant, as evident from the temperature decrease of the bulk solution until point A and the difference between inlet and outlet temperatures of the coolant. Latent heat of crystallization was released into the bulk solution during nucleation, causing a temperature rise (A). The formation of ice and salt crystals in the bulk also caused an increase in the heat transfer resistance on the process side (α_b). Because of the large temperature difference between coolant and bulk solution, some of the heat of crystallization was released directly to the coolant which resulted in an increase in the heat transfer rate and coolant outlet temperature (C). An insulating ice scale layer formed on the inside of the crystallizer wall at point D, providing resistance to heat transfer. Once scaling occurred, the description of the overall heat transfer coefficient (U_o), given by Equation 2.8, must be modified, to include the additional resistance provided by the ice layer. The overall heat transfer coefficient is now reduced, and is described by Equation 6.1:

$$\frac{1}{U_o} = \frac{1}{\alpha_b} + \frac{1}{\alpha_{wall}} + \frac{1}{\alpha_{cm}} + \frac{1}{\alpha_{ice}} \qquad 6.1$$

where α_b, α_{wall}, and α_{cm} are the heat transfer coefficients of the bulk solution, wall and cooling medium and α_{ice} is the heat transfer coefficient of ice. In addition to the increase in heat transfer resistance, remaining supersaturation was still being consumed within the bulk solution at point B, contributing to the temperature rise. **The induction time for ice scale formation was defined as the time between nucleation (A) and ice layer formation (B)[1],** which was approximately 66 minutes for the experimental run depicted in Figure 6.1.

[1] The term 'induction time' has been used in various ways in previous literature and has not been unequivocally defined. In crystallization theory, induction time generally refers to the rate of initial nucleation in the bulk solution; while in scaling theory induction time generally refers to the rate of initial nucleation on a cooled

During the induction time, the rate of heat release from crystallization was approximately equal to the heat removal rate from the crystallizer, hence the stable bulk temperature. Due to the thorough insulation of the crystallization vessel, as described in Section 5.2.1, heat losses were assumed negligible. The sensible heat of the feed stream was kept to a minimum through pre-cooling. The temperature probe had to be placed slightly below the crystallization zone, to accommodate the rotational movement of the scrapers, as discussed in Section 5.2.2. In this uppermost part of the lower separation zone where the temperature probe was placed, heat was released by the consumption of residual supersaturation but cooling did not occur; therefore, the measured bulk temperature during the suspension crystallization period was slightly above the eutectic temperature of the solution. This temperature is referred to simply as the bulk temperature in the remainder of the document.

6.1.2 Visual observations

Visual observation of both initial nucleation and scale layer formation supported the interpretation of the temperature response discussed in Section 6.1.1. During all experiments, nucleation was observed simultaneously in the bulk solution and on the cooled wall, when the bulk temperature reached the upper bound of the metastable zone. It was expected that heterogeneous nucleation on the wall would precede nucleation in the bulk solution, due to the lower free energy of formation for heterogeneous nucleation as well as the colder temperature of the wall as compared to the temperature of the bulk. However, throughout the experimental work, this was not the case. It is possible that dust particles in solution provided surface area for heterogeneous nucleation within the bulk, thereby prompting simultaneous heterogeneous nucleation on the wall and in the bulk solution. Another possibility is that heterogeneous nucleation occurred first in areas on the wall that could not be seen because of the insulation requirements of the crystallizer. Secondary nucleation then followed in quick succession, which resulted in simultaneous visual observation.

Following initial nucleation, a thin layer of ice was observed to grow on the wall. Scraper action was successful in removing the ice crystals and no meaningful impedance of heat transfer occurred, as can be seen from the temperature response in Figure 6.1. Removal of ice crystals continued, until, after approximately two minutes, ice nucleation and growth on the wall ceased. The start-up period in which initial nucleation and growth occur are associated

---

surface. Throughout this dissertation, induction time refers to the time period between initial nucleation and the formation of an ice scale layer on the cooled surface.

with the maximum supersaturation and lowest magma density in the bulk solution. If scraper action was successful in controlling scaling during this unsteady start-up stage, based on information from systematic studies currently available, scaling should not be a problem during further operation. However, in the current experimental work, seeding was not employed, prompting the formation of large amounts of small crystals during primary nucleation. As such, the ice surface area available for secondary nucleation and growth in the bulk solution, just after initial nucleation, was high. It is possible that the availability of this large surface area lessened the scaling tendencies during this period, an advantage that was not taken into consideration in relevant literature (Pronk et al., 2005; Vaessen et al., 2002).

After the initial ice growth on the wall had ceased, an induction time was observed, during which the wall remained seemingly free of ice. The possibility exists that a thin ice layer remained within the surface roughness of the glass vessel, and could not be observed due to the semi-transparent nature of ice, as was also postulated by Vaessen and co-workers (2003b). However, if in existence, this thin ice layer did not grow meaningfully in thickness or have a notable effect on heat transfer. During this period, ice accumulated in the bulk solution, providing surface area for secondary nucleation and growth.

The current experimental work was done at the high end of temperature driving forces, conditions which are associated with a high steady state magma density. The accumulation observed during the induction time was ascribed to the system not having achieved its steady state density yet. From visual observation, macroscopic mixing in the crystallizer was not impaired by the solids content during the majority of the induction time. It can, therefore, be assumed that supersaturation distribution in the crystallizer was sufficient and together with the availability of ice surface, explains the decreased tendency for ice to grow on the cooled wall. Adhesion and subsequent growth of ice were, however, observed on the scraper blades. Since the scrapers were in direct contact with the cooled wall and rotating through the colder boundary layer, subcooling of the blades occurred. The solid, unscraped surface of the blades provided ideal conditions for ice accumulation, as also observed by Ganiaris and co-workers (1969) during their pilot scale work. Although the work of Ganiaris and co-workers (1969) involved direct contact between impeller blades and refrigerant, the mechanism of ice accumulation on a subcooled, unscraped surface was similar.

It was observed that a rapid build-up of magma density in the crystallizer coincided with short induction times. Towards the end of the induction time, solids content in the crystallizer was notably impairing the ability of the scrapers to distribute supersaturation from the wall into the bulk solution. A high supersaturation developed at the wall, as a result of the obstruction

of radial fluid flow. At the end of the induction time, the high supersaturation prompted extremely rapid formation of a thick scale layer, which remained on the wall. At this point the strength of the ice layer exceeded the maximum rotational torque of the scraper motor and scrapers were stuck within the ice layer.

6.1.3 Summary of competing effects

In a scraped wall, eutectic freeze crystallizer, fluid of eutectic temperature is brought into contact with the cooled crystallizer wall, with every scraper pass. The variation of the fluid temperature in the vicinity of the wall with time, is shown in Figure 6.2, where the lowest temperature occurs between scraper passes and the highest temperature just after every scraper pass. At a critical value of magma density, solids in the crystallizer start to obstruct radial fluid movement. This results in a lower average temperature in the vicinity of the wall over a rotational cycle, as depicted in Figure 6.2.

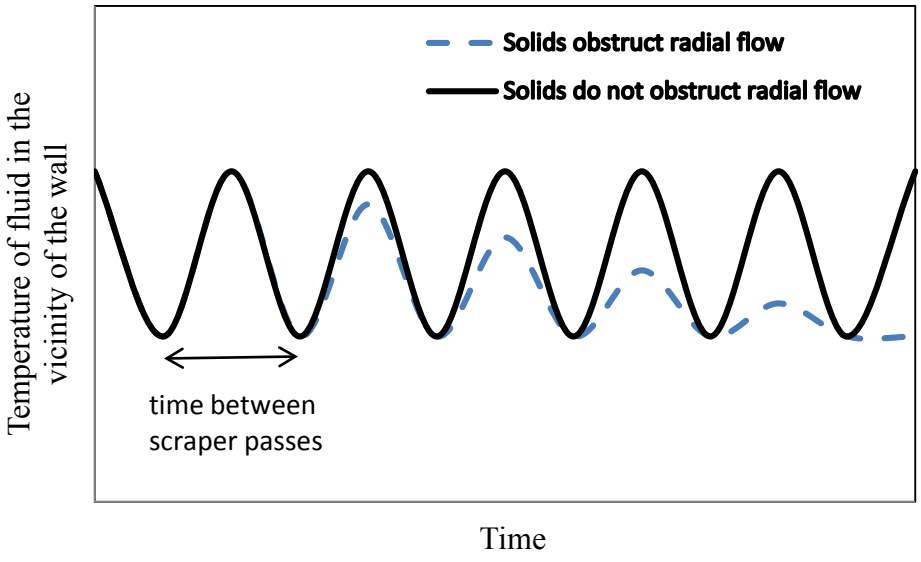

Figure 6.2: Qualitative representation of wall temperature in a scraped wall crystallizer

The availability of ice in the bulk solution serves as surface area for secondary nucleation and growth, lessening ice scaling on the cooled crystallizer wall. However, in certain systems, the steady state magma density is higher than the value required to obstruct radial fluid flow. In these systems, during the period where magma density is increasing, scaling will occur shortly after the critical value of magma density has been reached. The critical value is dependent on the crystallizer configuration, mixing regimes and nature of the solution. In systems where vigorous mixing occurs, the critical magma density will be much higher than in systems where mixing is

poor. The competing effects of magma density on scaling behaviour are qualitatively shown in Figure 6.3.

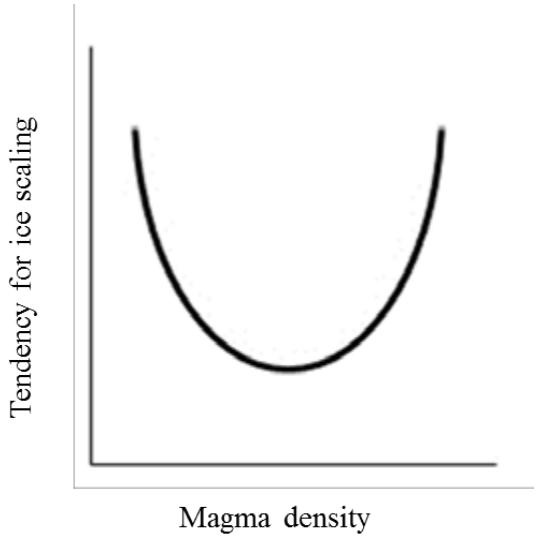

Figure 6.3: Qualitative relationship between scaling and magma density

6.2 Driving force for heat transfer

6.2.1 Variation in general trends

At heat transfer driving forces of 8.6 °C and 13.4 °C, visual observations were as described in Section 6.1.2. At a driving force of 15.8 °C, however, a thin, but visible layer of ice grew on the cooled wall during the first two minutes after initial nucleation and was never scraped off. The scrapers simply rotated on top of the ice layer, restricting its growth. The formation of this visible layer was attributed to the very high supersaturation that developed at the wall during application of the highest driving force investigated. Layer growth occurred at a very fast rate and although this ice layer was too thin to overcome the rotational torque of the scraper motor and result in process failure, it was thick enough to be visible and strong enough to remain on the wall.

This ice layer was not considered as scaling as it did not grow to a thickness which resulted in meaningful impairment of the rate of heat transfer or process failure. Although the ice layer did provide an additional resistance to heat transfer, visual observations indicated a similar build-up of magma density as observed at the other temperature driving forces. After an induction time, rapid formation of a thick scale layer occurred.

6.2.2 Effect of heat transfer driving force on induction time

The effect of the driving force for heat transfer on the onset time for scaling in a binary eutectic Na_2SO_4-H_2O solution is shown in Figure 6.4, at a constant scraper speed of 10.7 rpm.

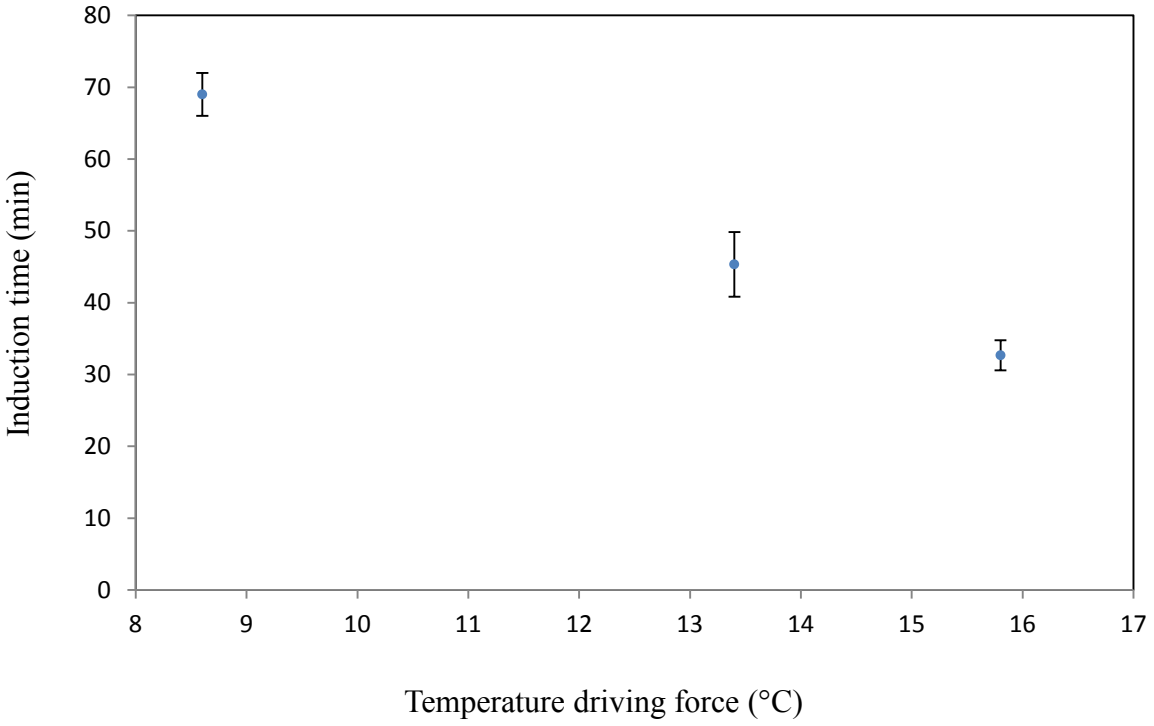

Figure 6.4: Influence of the driving force for heat transfer on induction time for the formation of an ice scale layer

A decrease in induction time was observed with an increase in heat transfer driving force. The decrease in induction time per unit change in temperature driving force became more pronounced towards the higher end of driving forces investigated.

The driving force for heat transfer affect scaling behaviour by influencing the rate of heat transfer from the bulk solution to the coolant as well as the supersaturation in the vicinity of the wall. The average heat transfer rates per unit surface area, during the induction time, is shown in Table 6-1, as calculated using Equation 2.6, at constant scraper speed of 10.7 rpm. Appendix B can be consulted for an example of the calculation. At higher heat transfer rates associated with higher driving forces, the total rate of crystallization is higher which generally results in a higher steady state magma density and a faster build-up thereof. Therefore, the system moves towards the critical magma density where fluid flow is impaired and scaling ensues, as discussed in Section 6.1.3.

Table 6-1: Heat transfer rates at varying driving force

Driving force for heat transfer (°C)	Heat transfer rate (W/m^2)
8.6	1087
13.4	1487
15.8	2004

In addition to increasing the total rate of crystallization, a higher driving force for heat transfer results in a more rapid recovery of the thermal boundary layer between scraper passes. This decreases the average temperature in the vicinity of the wall over a rotational cycle which increases the rate of crystallization in the vicinity of the wall. The higher undercooling further favours nucleation of large amounts of small crystals, as opposed to the growth of larger ones. A higher local rate of magma density build-up contributes to moving the system towards the critical magma density where fluid flow is impaired and scaling ensues, as discussed in Section 6.1.3.

Although previous systematic investigations into the relationship between the driving force for heat transfer and scaling behaviour were limited to time frames within 15 minutes of reaching the conditions under study, Vaessen and co-workers (2003a), Van der Ham and co-workers (2004) as well as Genceli and co-workers (2005) all reported increased scaling tendencies at higher driving forces. This relationship is, therefore, consistent with relevant literature and is also in accordance with what was logically expected.

6.3 Scraper speed

6.3.1 Variation in general trends

Over the complete range of temperature driving forces investigated, the scaling behaviour at a scraper speed of 2.1 rpm differed from the behaviour at higher scraper speeds. The temperature variation with time, during a single experimental run at a scraper speed of 2.1 rpm and a driving force for heat transfer of 8.6 °C, is shown in Figure 6.5. Point A indicates the bulk temperature response to nucleation; point B indicates the bulk temperature response to scale layer formation and point C, the increase in temperature of the coolant, associated with an increase in heat transfer from the crystallizer.

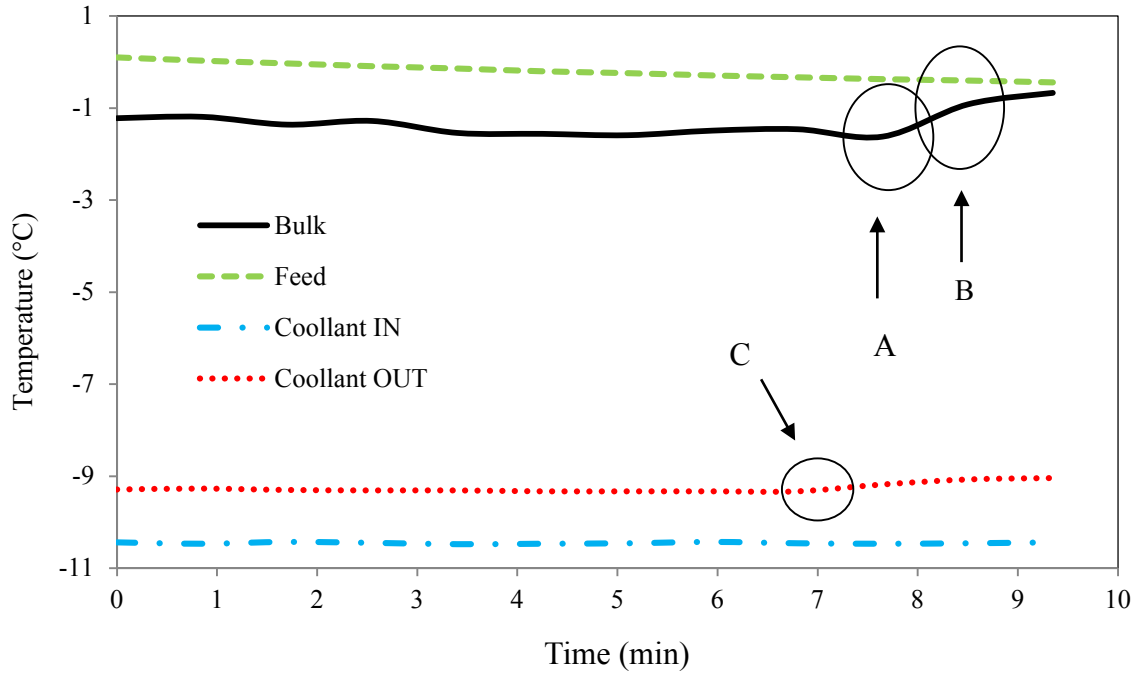

Figure 6.5: Scale formation during EFC of a binary Na_2SO_4-H_2O solution at a scraper speed of 2.1 rpm

Visual observation of nucleation coincided with the increase in the coolant outlet temperature at point C, while a delay of approximately 30 seconds occurred between point C and the response of the bulk solution temperature at point A. The rate of temperature increase at points A and C was less, as compared to the rate of temperature increase during initial nucleation at higher scraper speeds. At a scraper speed of 2.1 rpm, the rate of heat transfer before nucleation was lower and once nucleation was observed, movement of the suspension indicated poor mixing within the crystallizer. This resulted in a higher supersaturation in the vicinity of the wall and a much lower supersaturation in the centre of the crystallizer. The lower heat transfer rate and maldistribution of supersaturation resulted in a lower overall rate of crystallization, hence the lag in temperature response and decrease in the rate of the response once it did occur.

Nucleation and growth of ice were observed on the wall after every scraper pass and within a very short time of less than 2 minutes, an ice scale layer with sufficient strength to overcome the rotational torque of the scraper motor had formed. As can be seen from Figure 6.5, an induction time, during which the bulk temperature remained constant, was not observed. The maximum supersaturation present during initial nucleation together with the limited availability of ice surface area in the bulk solution, inefficient mixing and a time of seven

seconds between scraper passes, resulted in ice scaling within the start-up period. At scraper speeds of 6.4 rpm and 10.7 rpm, the temperature variation with time as well as visual observations were as described in Section 6.1.

6.3.2 Effect of scraper speed on induction time

The combined results of the experimental work done on the relationship between scraper speed and induction time for ice scale formation are shown in Figure 6.6. Reproducibility of results was good, as shown by error bars from experiments done in triplicate.

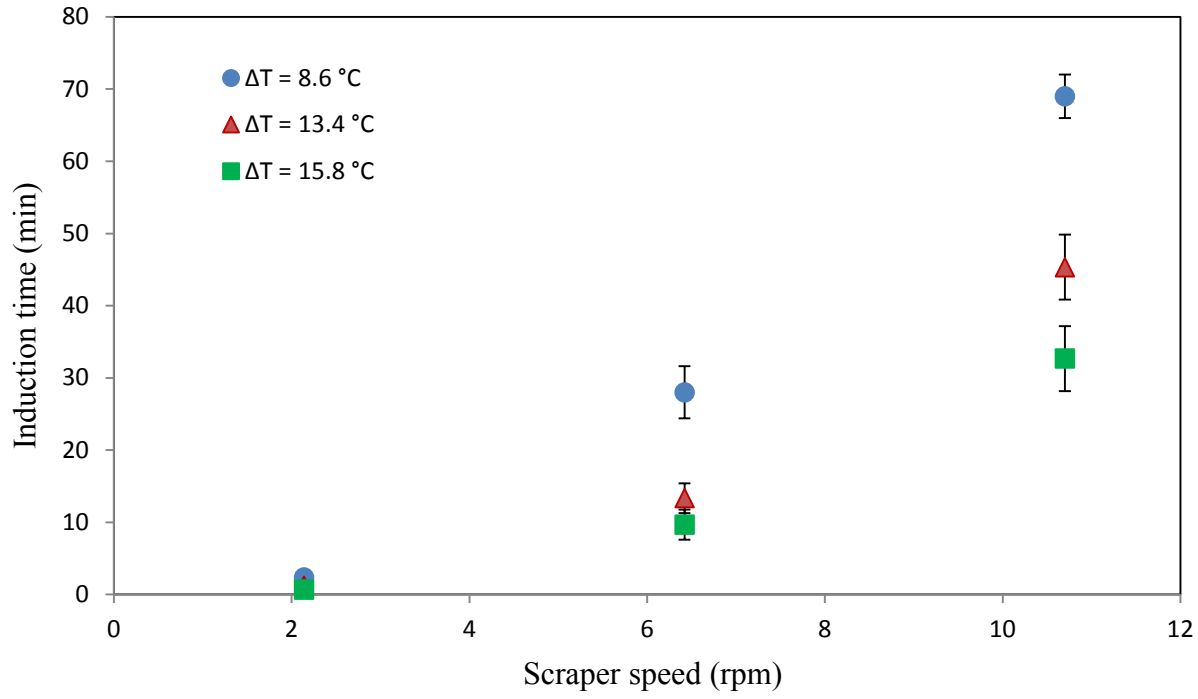

Figure 6.6: Induction time for the formation of an ice scale layer at varying scraper speed

Induction time showed a clear increase with an increase in scraper speed, at constant driving force for heat transfer. At larger driving forces, the rate of increase of induction time with scraper speed plateaued. Reproducibility of the results was very good, which was unexpected given the stochastic nature of primary nucleation and the variance in induction times loosely reported by Van der Ham and co-workers (2004). Throughout the range of driving forces, visual observation showed a more uniform build-up in magma density at faster scraper speeds, while adhesion and growth of ice on scraper blades were less severe.

Another representation of the same results is shown in Figure 6.7, indicating the relationship between induction time and the time between scraper passes, a design variable which can be applied to crystallizers of different configuration to the one used in the current work. The time between scraper passes is the inverse of the rotational scraper speed, taking into account the number of scraper arms used.

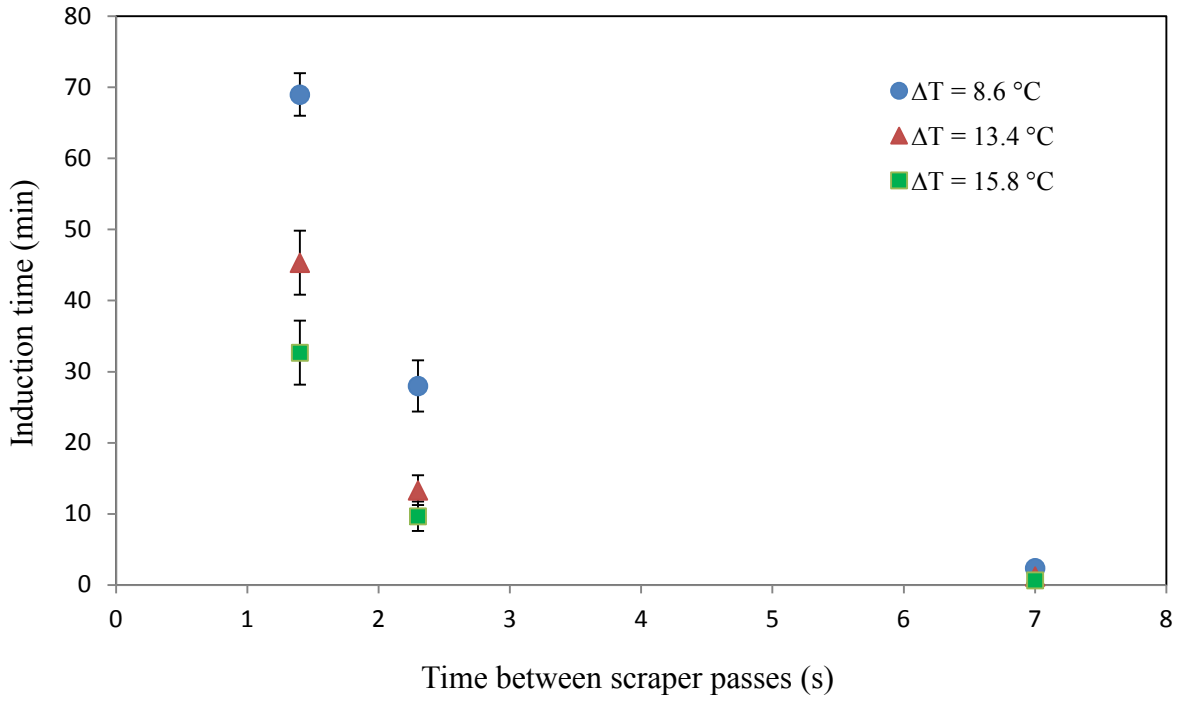

Figure 6.7: Induction time for the formation of an ice scale layer at varying time between scraper passes

Based on the reproducibility of the results, as shown by error bars in Figure 6.6 and Figure 6.7, primary nucleation did not have a significant influence on the rate of solids build-up and scaling behaviour. Had this been the dominant factor, a higher variance in results would have been expected. The rotational scraper speed affected scaling behaviour by influencing the undercooling at the wall, the rate of heat transfer from the bulk solution to the coolant and fluid flow at the wall and scraper blades.

With every scraper pass, the thermal boundary layer is removed, while the extent of its recovery between passes is dependent on the time between passes. At higher scraper speeds, the boundary layer is removed more frequently and it is possible that only partial recovery occurs between passes. Therefore, over a rotational cycle, the average temperature in the vicinity of the wall is higher at faster scraper speeds. A higher average temperature, or lower

undercooling, explains the slower build-up of magma density that was observed in the vicinity of the wall, which resulted in longer induction times.

At higher scraper speeds, the average heat transfer rate during the induction time was higher, as shown in Table 6-2. Values in Table 6-2 were calculated using Equation 2.6, at a constant driving force for heat transfer of 13.4 °C. At the slowest scraper speed of 2.14 rpm, no appreciable induction time was observed and the heat transfer rate represents heat transfer during initial nucleation.

Table 6-2: Heat transfer rates at varying scraper speed

Scraper speed (rpm)	Heat transfer rate (W/m^2)
2.14	1287
6.42	1317
10.70	1487

Even though the total rate of heat transfer was higher at faster scraper speeds (Table 6-2), and therefore, the total rate of crystallization more, the better distribution of solids resulted in a delay in the time between nucleation and impairment of radial fluid flow. Induction times were, therefore, longer at faster scraper speeds, as indicated in Figure 6.6.

The adhesive behaviour of ice on solid surfaces is also affected by scraper speed. During the induction time, the high solids density in the crystallizer could have resulted in the solution exhibiting dilatant rheological behaviour, as also observed by Tähti (2004) while investigating melt crystallization in a scraped surface crystallizer. Solutions with a high solids content often exhibit this behaviour, in which an increase in either fluid velocity or solids density cause an exponential increase in shear stress at the solid surface (Hafaiedh, 1988). This behaviour had different effects on the cooled wall and the scraper blades. At the cooled wall, at both high and low driving forces for heat transfer, the local supersaturation at the wall was high, as discussed in Section 6.2.2, resulting in a high local solids density and, therefore, a high shear stress. Higher scraper speeds resulted in an increase in shear stress due to an increase in lateral fluid flow, explaining the longer induction times observed. However, a plateau in the rate of induction time increase with scraper speed, at higher driving forces for heat transfer was not expected. In contrast, the back of the scraper blades, which protruded

into the bulk solution, experienced a high solids density at high heat transfer driving forces but at low driving forces the build-up of magma density in the bulk solution was slower due to the lower rate of heat transfer. At high driving forces, the change in shear stress with change in scraper speed was, therefore, solely due to the change in fluid velocity. However, at low driving forces, better distribution of solids at faster scraper speeds resulted in an increased magma density at the back of the scraper blades which, in combination with the effect of increased lateral flow caused an exponential increase in shear stress. Adhesion and growth of ice on the back of the blades were, therefore, less severe which prolonged the time until the critical magma density was reached. This explained the higher rate of increase of induction time with scraper speed at lower driving forces for heat transfer.

From the time dependent scaling behaviour depicted in Figure 6.6, it is clear that scaling is a function of macroscopic variables within the crystallizer, such as magma density, which keep on changing long after the temperature in the crystallizer reach a pseudo steady state. Induction times, for all but the slowest scraper speed, were more than 10 minutes, which is the time interval studied in relevant literature on EFC of inorganic salt solutions (Vaessen et al., 2002, Pronk et al., 2005). Pronk and co-workers (2005) reported an increase in scaling behaviour with an increase in scraper speed, during crystallization of an aqueous potassium nitrate solution, a result which disagrees with the findings of the current work. Lakhdar and co-workers (2005) reported on steady state experiments at high rotational speeds, using aqueous sucrose and ethanol solutions at dilute concentrations. Although not directly comparable with the current work due to the organic nature of the solutions, dilute solute concentrations and high rotational speeds investigated, Lakhdar and co-workers (2005) observed a decrease in scaling tendencies with increasing scraper speed similar to the decrease in time-dependant scaling behaviour that was observed with an increase in scraper speed in the current work.

6.4 Solute type and concentration

The induction time for scale formation during EFC of a $NaSO_4$-H_2O solution of varying impurity content is shown in Figure 6.8. Repeatability of results was satisfactory, as shown by error bars in Figure 6.8, from experiments done in triplicate. The scraper speed and driving force for heat transfer were kept constant, at 6.4 rpm and a 13.4 °C; as such the data at zero impurity content corresponds to the data under similar conditions in Figure 6.6.

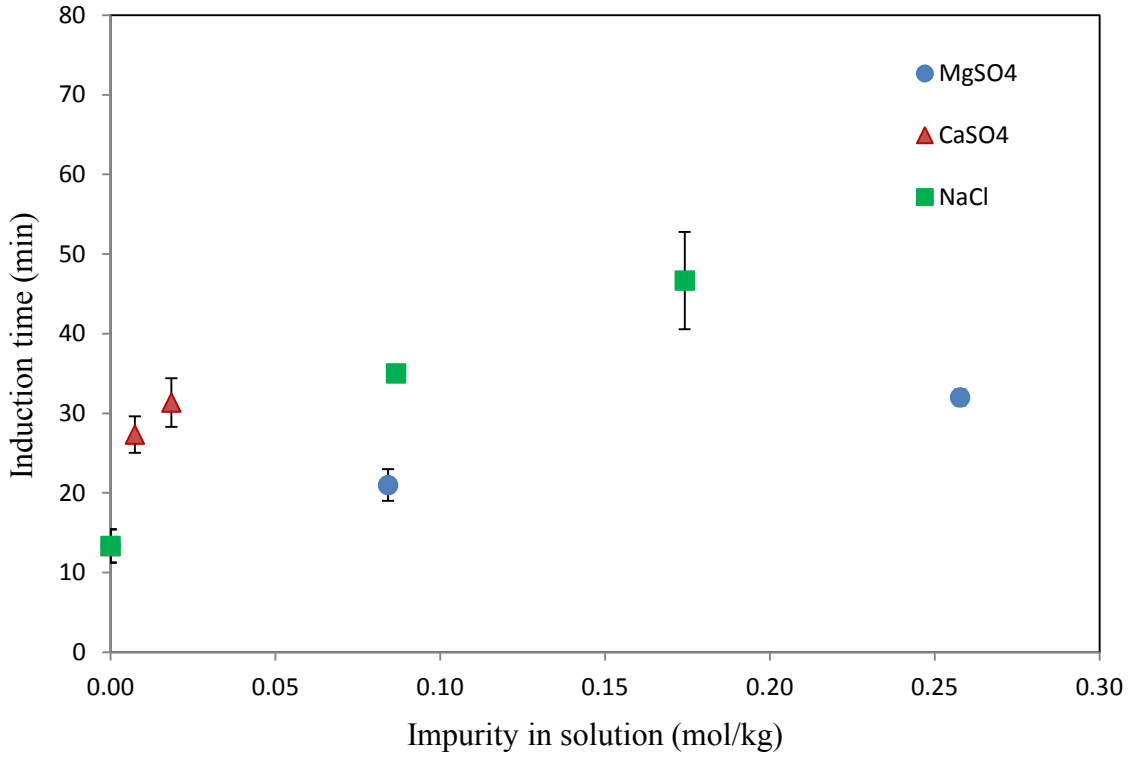

Figure 6.8: Induction time for the formation of an ice scale layer during EFC of a binary $NaSO_4$ solution of varying impurity content

6.4.1 Solute type

The presence of small quantities of impurities in the eutectic Na_2SO_4-H_2O system resulted in increased induction times, unique to each dissolved ionic species, as shown in Figure 6.8. Calcium sulphate is only slightly soluble in water at -1.15 °C. In the concentration range from 0.01 to 0.02 mole $CaSO_4$ per kilogram solution (mol/kg) an increase of 400 minutes per unit molality (min·kg/mol) in induction time was observed. Sodium chloride resulted in a 146 min·kg/mol increase, within a concentration range from 0.09 mol/kg to 0.17 mol/kg, while magnesium sulphate, in concentrations from 0.08 mol/kg to 0.26 mol/kg resulted in a 61 min·kg/mol increase. From visual observations, it was clear that the adhesion of crystals on scraper blades was delayed in the presence of impurities, and when adhesion did occur, subsequent growth and accumulation of crystals behind the blades also happened at a slower rate.

The increase in induction times observed in the presence of impurities, as shown in Figure 6.8, can be attributed to several factors. Impurities in solution affect induction times by depressing the freezing point of the solution and thereby decreasing the driving force for heat

transfer at fixed coolant temperature. Furthermore, solute molecules must diffuse away from the existing ice layer to allow growth and electrostatic interaction between ionic impurities and the ice surface affect the adhesive force of ice on both the cooled wall and scraper blades.

6.4.1.1 Effect of freezing point depression

The freezing point and pH of a eutectic Na_2SO_4-H_2O solution of varying impurity content is given in Table 6-3, as calculated using thermodynamic modelling software OLI Studio 9.2 (2015). Differences in the driving force for heat transfer due to freezing point depression (FPD) between the pure Na_2SO_4-H_2O solution and those containing impurities range from 0.01 °C to 0.46 °C. These are very small changes compared to the driving force of 13.4 °C applied through control of the coolant temperature. For comparison, $CaSO_4$ at a concentration of 0.01 mol/kg caused a twofold increase in induction time, at a reduction of 0.01 °C in driving force due to FPD. A twofold increase in induction time for the pure eutectic Na_2SO_4-H_2O system was only achieved at a 5 °C reduction in driving force through adjustment of the coolant temperature, as shown in Figure 6.6. These two factors cannot be compared directly because FPD affects supersaturation for ice throughout the solution, while the driving force applied by adjustment of the coolant temperature decrease radially due to the heat transfer resistances of the wall and process liquid. However, the magnitude of the increase in induction time in the presence of impurities suggests that factors other than FPD also contribute to the decrease in scaling behaviour.

Table 6-3: Freezing point and pH of a eutectic Na_2SO_4-H_2O solution of varying impurity content (OLI Systems Inc, 2015)

Impurity (mol/kg)	Freezing point (°C)	pH
Zero	-1.14	7.6
0.01 $CaSO_4$	-1.15	7.6
0.02 $CaSO_4$	-1.16	7.6
0.09 NaCl	-1.31	7.6
0.17 NaCl	-1.50	7.6
0.08 $MgSO_4$	-1.29	7.5
0.26 $MgSO_4$	-1.60	7.3

6.4.1.2 Differences in behaviour between $CaSO_4$ and $MgSO_4$ impurities

The specific induction times observed in the presence of impurities can be explained by unique electrostatic interactions between solute ions and the solid ice surface. More aggressive interaction could cause a larger decrease in the density of hydrogen bonding in the ice lattice, resulting in lower adhesive strength. It was expected that Mg^{2+} would have a more significant effect on scaling behaviour than Ca^{2+} due to the size of the ionic radii and influence on the solution pH. Calcium ions have an ionic radius of 1.00 Å, while magnesium ions are smaller, with an ionic radius of 0.72 Å (Lide, 2004). Larger ions cannot come as close to the dipole moments at the ice surface as smaller ions can and would, therefore, be expected to have a lesser influence on the electrostatic potential of the surface. However, this was not the case, as $MgSO_4$ did not have a more significant effect on induction time as $CaSO_4$. It is possible that the size of ionic radius affect scaling in a way opposite to expectation. At similar charge but smaller radius, Mg^{2+} has a higher charge density than Ca^{2+}. The higher charge density corresponds to a higher enthalpy of hydration, with the energy necessary to remove Mg^{2+} from a water molecule being 1920 kJ/mol while that of Ca^{2+} is only 1650 kJ/mol (Royal Society of Chemistry, 2006). A higher degree of hydration of Mg^{2+} might prevent interaction of the ions with the ice layer surface, thereby limiting the effect of Mg^{2+} on scaling behaviour.

As seen in Table 6-3, thermodynamic modelling showed that the presence of $MgSO_4$ causes a decrease in the pH of the solution and therefore, an increase in the H_3O^+ concentration. Vaessen (2003) observed that in acidic solutions, the presence of higher concentrations H_3O^+ decreased scaling behaviour. It was postulated that when ice forms from electrolyte solutions, an uneven charge distribution might occur within the ice structure, due to ionic interaction with solute molecules. With time, water molecules dissociate to neutralize the maldistribution of charge within the ice lattice and a higher concentration of H_3O^+ in solution can increase the rate of neutralization. If the postulation made by Vaessen (2003) is applicable at small concentrations of hydronium ions, $MgSO_4$ should show longer induction times by virtue of the slightly lower pH and lowering effect of electrostatic interaction on the adhesive strength of ice. However, this was not the case, as $MgSO_4$ did not have a more significant effect on induction time as $CaSO_4$.

The diffusivities of Ca^{2+} and Mg^{2+} in water are very similar, with diffusion coefficients of 0.792 nm^2/s and 0.706 nm^2/s (Samson, Marchand & Snyder, 2003), therefore, differences in

induction times between the two species cannot be attributed to the speed with which ions diffuse away from the growing ice layer.

6.4.1.3 Effect of NaCl impurity

The threefold increase in induction time observed in the presence of 0.17 mol/kg NaCl can be attributed to the presence of chloride ions. Since the eutectic $NaSO_4$-H_2O solution already contains 0.72 molNa^+/kg, it is unlikely that further increase of 0.17 molNa^+ /kg would have such a significant effect. In addition to this, Na^{2+} is crystallizing out of solution as Na_2SO_4-H_2O, due to the proximity to the eutectic point, which reduces the Na^{2+} concentration and therefore, its effect on scaling behaviour. The influence of NaCl on scaling behaviour is much larger than would be expected based on its freezing point depression, shown in Table 6-3, and subsequent increase in driving force for heat transfer. Chlorine has a high electronegativity of 3, as compared to the much lower electronegativities of sodium at 0.9, calcium at 1.0 and magnesium at 1.2. In ionic form, the chloride ion strongly attracts an additional electron; which might allow more aggressive interaction with the dipole moments at the ice surface, and therefore, lowering of the attractive force between ice and other solid surfaces.

Although the diffusivity of Cl^- in water is high, with a diffusion coefficient of 2.032 nm^2/s (Samson et al., 2003); attractive forces between the electropositive ice surface and negative chloride ions might result in the growth rate of the ice layer being diffusion limited. In addition to that, Cl^- has a low enthalpy of hydration of 338 kJ/mol (Royal Society of Chemistry, 2006). A lower degree of hydration will enhance interaction of ions with the ice surface and further limit diffusion of ions away from the growing ice layer.

6.4.2 **Concentration**

For all the investigated solute types, an increase in solute concentration resulted in an increase in induction time. The solute types that had a larger influence on induction time at the smallest measured concentration also showed a higher rate of increase in induction time with concentration, as seen in Figure 6.8.

The longer induction times observed at higher solute concentrations were attributed to the increased resistance to ice layer growth provided by mass transfer of solute molecules away from the ice-liquid interface. At higher solute concentrations, the solute molecules in solution

provide more resistance to the movement the rejected molecules away from the growing ice front.

In the systematic study done by Vaessen and co-workers (2002), a decrease in scaling tendencies was observed with an increase in concentration for five binary aqueous electrolyte solutions. Vaessen and co-workers (2002) attributed the behaviour to the mass transfer limitation provided by solute molecules. Pronk (2006) went on to test the hypothesis by modelling the contributions of mass transfer, heat transfer and surface integration to the resistance to ice layer growth from a dilute aqueous NaCl solution. The modelling results showed that ice growth from NaCl solution is mass transfer controlled at concentrations above 0.2 mol%, which is well below the concentration range investigated in the current work. Although Na^{2+} is, in the current system, crystallizing out of solution, Cl^{-} still accumulate at the growing ice front and must still move away through diffusion. It is, therefore, reasonable to attribute the decrease in scaling tendencies with increase in concentration observed from impure $NaSO_4$-H_2O solutions, to an increase in the mass transfer limitation.

7 Conclusions

The formation of an ice scale layer on cooled crystallizer surfaces is an operational limitation during continuous eutectic freeze crystallization of aqueous electrolyte solutions. Ice scaling is prevalent during the application of large temperature driving forces associated with high production rates of ice and salt. This research focused on determining the induction time, defined as the time between initial nucleation and scale layer formation, where shorter induction times are associated with more severe scaling tendencies. The effect of the driving force for heat transfer, scraper speed and the solute type and concentration of inorganic electrolyte impurities in a binary eutectic Na_2SO_4-H_2O system was investigated.

The formation of an ice scale layer on cooled crystallizer surfaces during continuous EFC of an aqueous Na_2SO_4 solution occurred either during the period of initial nucleation or after an induction time during which the wall was clear of ice and the magma density in the crystallizer increased. Scaling during the initial nucleation period was attributed to a high supersaturation for ice crystallization and a lack of ice surface available in the bulk solution for secondary nucleation and growth. Scale formation after an induction time was characterized by extremely rapid ice layer formation and was ascribed to a high magma density which compromised the ability of the scrapers to distribute supersaturation and resulted in a high local supersaturation in the vicinity of the cooled wall.

A decrease in induction time was observed with an increase in the driving force for heat transfer. The shorter induction times at larger driving forces were attributed firstly to a lower wall temperature which promoted crystallization on the wall and secondly to a higher rate of heat transfer which promoted a fast build-up of magma density in the vicinity of the wall. The high magma density impaired radial fluid flow, resulting in a high local supersaturation at the wall.

Induction time showed an increase with an increase in scraper speed, at constant heat transfer driving force. With every scraper pass, fluid of eutectic temperature was brought into contact with the cold wall and magma was distributed from the wall into the bulk. The longer induction times at higher scraper speeds were attributed to the higher average temperature in the vicinity of the wall as well as a better distribution of magma within the crystallizer. Scraper blades experienced a higher shear stress due to the faster movement through the

solution as well as better magma distribution. Higher shear stress limited ice adhesion and subsequent growth on scraper blades which retarded local magma build-up and its inhibition of radial fluid flow.

The presence of small quantities of impurities in the eutectic Na_2SO_4-H_2O system resulted in increased induction times, specific to each dissolved ionic species. The specific induction times observed were explained by unique electrostatic interactions between solute ions and the electropositive ice surface. The extent to which ions in solution were able to interact with the ice surface had an influence on the adhesive properties of ice. Magnesium ions have a higher charge density and, therefore a higher enthalpy of hydration than calcium ions. A higher degree of hydration of Mg^{2+} possibly limited its effect on the ice surface which explained the differences in induction times observed in the presence of Ca^{2+} and Mg^{2+}. The highly electronegative chloride ions, with a low enthalpy of hydration were able to effectively interact with the ice layer surface, lessening the adhesivity of the ice layer. In addition to affecting adhesivity, the negatively charged chloride ions were attracted to the electropositive ice surface, which retarded solute diffusion away from the growing ice layer and therefore, limited ice layer growth.

For all the investigated solute types, an increase in solute concentration resulted in an increase in induction time. The longer induction times observed at higher solute concentrations were attributed to the increased resistance to ice layer growth provided by mass transfer of solute molecules away from the ice-liquid interface.

The qualitative trends observed during this research are applicable to crystallization of industrial brine streams, including neutralized acid mine drainage and hydrometallurgical effluents. Where indirect cooling is applied in scraped wall crystallization vessels, ice scaling tendencies are less during crystallization of impure aqueous solutions as compared to binary streams and can be further minimized by keeping the time between scraper passes below 1.5 seconds. Scaling is a function of the temperature driving force for heat transfer, where the benefits of prolonged steady state operation should be weighed against production rates at varying driving force.

8 Recommendations

The current research highlighted the importance of magma density and its effects on fluid flow and scaling behaviour in scraped eutectic crystallizers. Optical techniques can be used to measure magma densities below approximately 5 wt%, however, at higher densities, accurate techniques applicable to scraped wall crystallizers; especially hybrid crystallizer-separators are not available. With control strategies for crystallizers of industrial size in mind, there is a need to develop an easy-to-use measurement technique for the operational magma density.

Very limited information is available in literature on continuous EFC of real, multicomponent brines. The effect of impurities in the binary Na_2SO_4-H_2O system on scaling behaviour observed in the current research gives a positive indication that the problem of ice scaling might be less severe during EFC of multicomponent brines. However, the large variation in behaviour that was observed between solute types emphasize the need for laboratory scale research on real brines, taking into consideration that the composition of wastewater will vary with time in an industrial setup.

Eutectic freeze crystallization as well as cooling crystallization offers excellent opportunities for energy integration. In its simplest form, the ice product can be used to pre-cool the feed stream; alternatively, it can be used for refrigeration purposes in other industrial operations. An overall energy balance, including design alternatives for heat integration as well as comparison of energy usage at varying scraper speeds, mixing regimes, coolant temperatures and coolant flow rates will be beneficial for future designs.

9 References

Baehr, H.D. & Stephan, K. 1998. *Heat and mass transfer.* Berlin: Springer.

Chivavava, J. 2013. Effect of operating conditions on product quality in continuous eutectic freeze crystallization. M.Sc Thesis. University of Cape Town.

Cloete, T., Gerber, A. & Maritz, L. 2010. *A first order inventory of water use effluent production by SA industrial, mining and electricity generation sectors.* (Research report 1547/1/10). Pretoria: Water Research Commission.

Coetzee, C.B. 1976. *Mineral resources of the Republic of South Africa.* South Africa: The Survey.

De Goede, R. & De Jong, E.J. 1993. Heat transfer properties of a scraped-surface heat exchanger in the turbulent flow regime. *Chemical Engineering Science.* 48(8):1393-1404.

De Goede, R. 1988. Crystallization of paraxylene with scraped surface heat exchangers. Ph.D. Thesis. Delft University of Technology.

Denton, W.H., Smith, M.J.S., Klaschka, J.T., Forgan, R., Diffey, H.R., Rumary, C.H. & Dawson, R.W. 1974. Experimental studies on washing and melting ice crystals in the immiscible refrigerant freezing process. *Desalination.* 14(3):263-290.

Dirksen, J.A. & Ring, T.A. 1991. Fundamentals of crystallization: Kinetic effects on particle size distributions and morphology. *Chemical Engineering Science.* 46(10):2389-2427.

Dittus, F.W. & Boelter, L.M.K. 1985. Heat transfer in automobile radiators of the tubular type. *International Communications in Heat and Mass Transfer.* 12(1):3-22.

Estrin, J. 1970. *Secondary nucleation of ice in a suspension of crystals in turbulent cylindrical couette flow.* (Technical report 494). Washington, D.C.: United States Department of the Interior.

Fletcher, R. 1958. Size effect in heterogeneous nucleation. *The Journal of Chemical Physics.* 29(3):572-576.

Ganiaris, N., Lambiris, J. & Glasser, R. 1969. *Secondary refrigerant freezing desalting process: Operation of a 15, 000 GPD pilot plant.* (Research report 416). Oklahoma, USA: United States Department of the Interior.

Genceli, F.E. 2008. Scaling-up eutectic freeze crystallization. Ph.D. Thesis. Delft University of Technology.

Genceli, F.E., Gärtner, R. & Witkamp, G.J. 2005. Eutectic freeze crystallization in a 2nd generation cooled disk column crystallizer for $MgSO_4 \cdot H_2O$ system. *Journal of Crystal Growth.* 275(1):1369-1372.

Gunther, P. & Naidu, T. 2008. Mine water reclamation: Towards zero disposal. *Proceedings of the Biennial WISA Conference.* Johannesburg, South Africa.

Hafaiedh, A. 1988. *Computer modeling of the rheology of particulate suspensions.* (Technical report DOE/PC/70804-T5). New York, USA: Alfred University.

Halde, R. 1980. Concentration of impurities by progressive freezing. *Water Research.* 14(6):575-580.

Hossein, K. & Da-Wen, S. 2011. Water crystallization and its importance to freezing of foods: a review. *Trends in Food Science & Technology*. 22: 407-426.

Huige, N.J.J. 1972. Nucleation and growth of ice crystals from water and sugar solutions in continuous stirred tank crystallizers. Ph.D. Thesis. Eindhoven University of Technology.

Israelachvili, J.N. 2011. *Intermolecular and surface forces.* USA: Academic press.

Johnson, D.B. & Hallberg, K.B. 2005. Acid mine drainage remediation options: a review. *Science of the Total Environment.* 338(1):3-14.

Johnson, W.E. 1976. State-of-the-art of freezing processes, their potential and future. *Desalination.* 19(1):349-358.

Johnson, W.E. 1979. Indirect freezing. *Desalination.* 31(1):417-425.

Kakaç, S., Shah, R.K. & Aung, W. 1987. *Handbook of single-phase convective heat transfer.* New York: John Wiley & Sons.

Kashchiev, D. 2000. *Nucleation, Basic Theory with application.* Oxford, UK: Butterworth-Heinemann.

Koop, T., Luo, B., Tsias, A. & Peter, T. 2000. Water activity as the determinant for homogeneous ice nucleation in aqueous solutions. *Nature.* 406:611-614.

Lakhdar, M.B., Cerecero, R., Alvarez, G., Guilpart, J., Flick, D. & Lallemand, A. 2005. Heat transfer with freezing in a scraped surface heat exchanger. *Applied Thermal Engineering.* 25(1):45-60.

Lauda 2015. *Heat transfer liquids - Thermostats, circulation chillers, water baths.* Available: http://laudaonline.com/hosting/lauda/website_en.nsf/urlnames/DSJL-prosp_temperierfluess_2014/$file/Prospekt_Temperierfluessigkeiten_2014_web.pdf [2016, January 5].

Lewis, A., Seckler, M., Kramer, H. & van Rosmalen, G. 2015. *Industrial Crystallization: Fundamentals and Applications.* Cambridge, UK: Cambridge University Press.

Lide, D.R. 2004. *CRC handbook of chemistry and physics.* USA: CRC press.

Lorain, O., Thiebaud, P., Badorc, E. & Aurelle, Y. 2001. Potential of freezing in wastewater treatment: soluble pollutant applications. *Water Research.* 35(2):541-547.

Mersmann, A. 2001. *Crystallization technology handbook.* Basel, Switzerland: Marcel Dekker.

Mullin, J.W. 2001. *Crystallization.* Reed Educational and Professional Publishing Ltd.

Myerson, A.S. & Ginde, R. 2002. *Handbook of industrial crystallization.* Butterworth-Heinemann.

Nelson, S.A. 2011. *Ternary Phase Diagrams.* Available: http://www.tulane.edu/~sanelson/eens212/ternaryphdiag.pdf [2015, November 11].

OLI Systems Inc. 2015. *OLI Stream Analyser* [Computer software]. Version 9.2. New Jersey, USA.

Petrenko, V.F. 1993. *Electrical properties of ice.* (Special report ADA270432). Hanover, Germany: Cold Regions Research and Engineering Lab.

Pronk, P. 2006. Fluidized bed heat exchangers to prevent fouling in ice slurry systems and industrial crystallizers. Ph.D. Thesis. Delft University of Technology.

Pronk, P., Ferreira, C.A.I., Rodriguez, M.P. & Witkamp, G.J. 2005. Maximum temperature difference without ice-scaling in scraped surface crystallizers during eutectic freeze crystallization. *Proceedings of the 16th International Symposium on Industrial Crystallization.* Dresden, Germany.

Qin, F.G.F., Chen, X.D. & Farid, M.M. 2004. Growth kinetics of ice films spreading on a subcooled solid surface. *Separation and Purification Technology.* 39(2004):109-121.

Qin, F.G.F., Chen, X.D. & Russell, A.B. 2003. Heat transfer at the subcooled-scraped surface with/without phase change. *AIChE Journal.* 49(8):1947-1955.

Randall, D.G. 2010. Development of a brine treatment protocol using eutectic freeze crystallization. Ph.D. Thesis. University of Cape Town.

Rodriguez, P.M., Lewis, A.E. 2013. A novel stirred scraped wall crystallizer designed for melt and eutectic freeze crystallization. *Proceedings of the 17th International Conference on Crystal Growth and Epitaxy.* Warsaw, Poland.

Rodriguez, P.M. 2009. Physical aspects of scraped heat exchanger crystallizers: an application in eutectic freeze crystallization. Ph.D. Thesis. Delft University of Technology.

Rodriguez, P.M., Ravelet, F., Delfos, R., Derksen, J.J. & Witkamp, G.J. 2008. Measurement of flow field and wall temperature distribution in a scraped heat exchanger crystallizer.

Proceedings of the 5th European Thermal-Sciences Conference. Eindhoven, The Netherlands.

Royal Society of Chemistry 2006. *Hydration enthalpies of selected ions.* Available: http://www.rsc.org/Education/Teachers/Resources/Databook/ds_hydration_enthalpies.htm [2015, December 22].

Ryzhkin, I.A. & Petrenko, V.F. 1997. Physical mechanisms responsible for ice adhesion. *The Journal of Physical Chemistry B.* 101(32):6267-6270.

Samson, E., Marchand, J. & Snyder, K.A. 2003. Calculation of ionic diffusion coefficients on the basis of migration test results. *Materials and Structures.* 36(3):156-165.

Söhnel, O., Bravi, M., Chianese, A. & Mazzarotta, B. 1996. Growth kinetics of sodium perborate from batch crystallization. *Journal of Crystal Growth.* 160(3):355-360.

Statistics South Africa 2015. *Mid-year population estimates 2015.* (Report P0302). Pretoria, South Africa: Statistics South Africa.

Stepakoff, G.L., Siegelman, D., Johnson, R. & Gibson, W. 1974. Development of a eutectic freezing process for brine disposal. *Desalination.* 15(1):25-38.

Tähti, T. 2004. Suspension melt crystallization in tubular and scraped surface heat exchangers. Ph.D. Thesis. Martin Luther University of Halle Wittenberg.

Thomsen, K. 1997. Aqueous electrolytes: model parameters and process simulation. Ph.D. Thesis. Technical University of Denmark.

US Geological Survey 2015. *Mineral commodity summaries 2015: US Geological Survey.* (Report 196). Reston, Virginia: US Department of the Interior.

Ulrich, J. & Jones, M.J. 2006. Heat and Mass Transfer Operations-Crystallization. In *Chemical Engineering and Chemical Process Technology.* J. Bridgwater, M. Molzahn & R. Pohorecki, Eds. Oxford, UK: Encyclopedia of Life Support Systems Publishers. 1-31.

Ulrich, J. & Stelzer, T. 2011. Crystallization. In *Kirk-Othmer Encyclopedia of Chemical Technology.* Online ed. New York: John Wiley and Sons, Inc. 1-63.

Vaessen, R. 2003. Development of scraped eutectic crystallizers. Ph.D. Thesis. Delft University of Technology.

Vaessen, R., Seckler, M. & Witkamp, G.J. 2003a. Eutectic freeze crystallization with an aqueous KNO_3-HNO_3 solution in a 100-L cooled-disk column crystallizer. *Industrial & Engineering Chemistry Research.* 42(20):4874-4884.

Vaessen, R.J.C., Janse, B.J.H., Seckler, M.M. & Witkamp, G.J. 2003b. Evaluation of the performance of a newly developed eutectic freeze crystallizer: scraped cooled wall crystalIizer. *Chemical Engineering Research and Design.* 81(10):1363-1372.

Vaessen, R.J.C., Himawan, C. & Witkamp, G.J. 2002. Scale formation of ice from electrolyte solutions on a scraped surface heat exchanger plate. *Journal of Crystal Growth.* 237–239(3):2172-2177.

Van der Ham, F., Seckler, M.M. & Witkamp, G.J. 2004. Eutectic freeze crystallization in a new apparatus: the cooled disk column crystallizer. *Chemical Engineering and Processing: Process Intensification.* 43(2):161-167.

Van der Ham, F. 1999. Eutectic freeze crystallization. Ph.D. Thesis. Delft University of Technology.

Volland, W. 2011. *Intermolecular forces dipole-dipole, London forces, hydrogen bonding versus covalent bonds.* Available: http://www.800mainstreet.com/08/0008-0012-interforce.html [2015, November 23].

World Bank Database 2015a. *Average precipitation in depth.* Available: http://data.worldbank.org/indicator/AG.LND.PRCP.MM [2016, January 4].

World Bank Database 2015b. *Renewable internal freshwater resources per capita.* Available: http://data.worldbank.org/indicator/ER.H2O.INTR.PC [2016, January 4].

Zwietering, T.N. 1958. Suspending of solid particles in liquid by agitators. *Chemical Engineering Science.* 8(3):244-253.

APPENDIX A

Temperature variation with time for an experimental run during EFC of a binary Na_2SO_4-H_2O solution, at a driving force of 8.6 °C and scraper speed of 6.42 rpm:

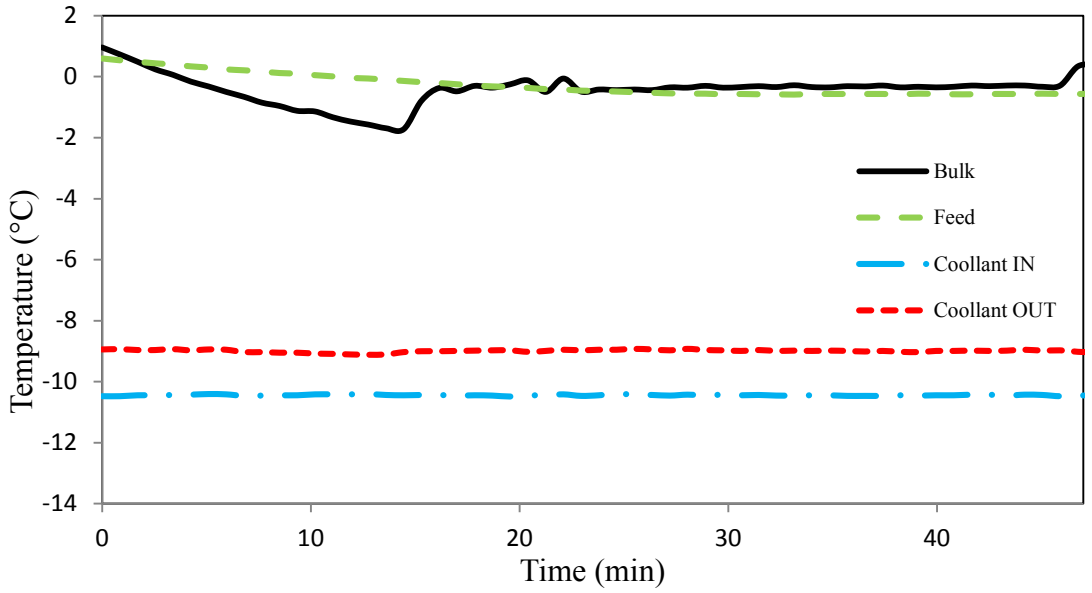

Figure A.1: Heat transfer driving force of 8.6 °C, scraper speed of 6.42

Temperature variation with time for an experimental run during EFC of a binary Na_2SO_4-H_2O solution, at a driving forces of 15.8 °C and scraper speed of 10.7 rpm:

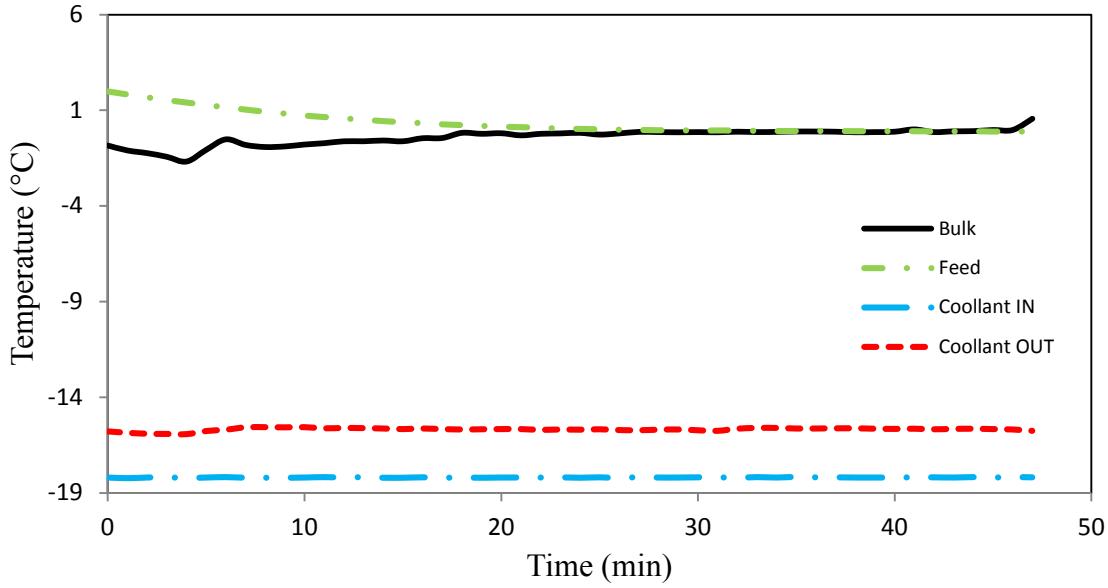

Figure A.2: Temperature driving force of 15.8 °C, scraper speed of 10.7 rpm

Temperature variation with time for experimental runs during EFC of a binary Na_2SO_4-H_2O solution, at scraper speeds of 2.14 rpm, 6.42 rpm and 10.7 rpm:

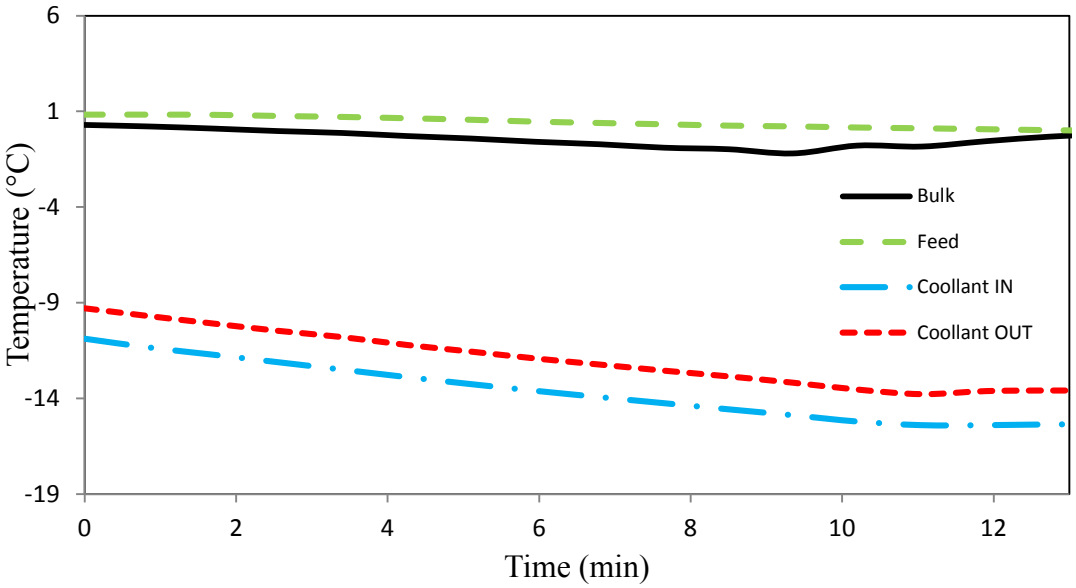

Figure A.3: Heat transfer driving force of 13.4 °C, scraper speed of 2.14 rpm

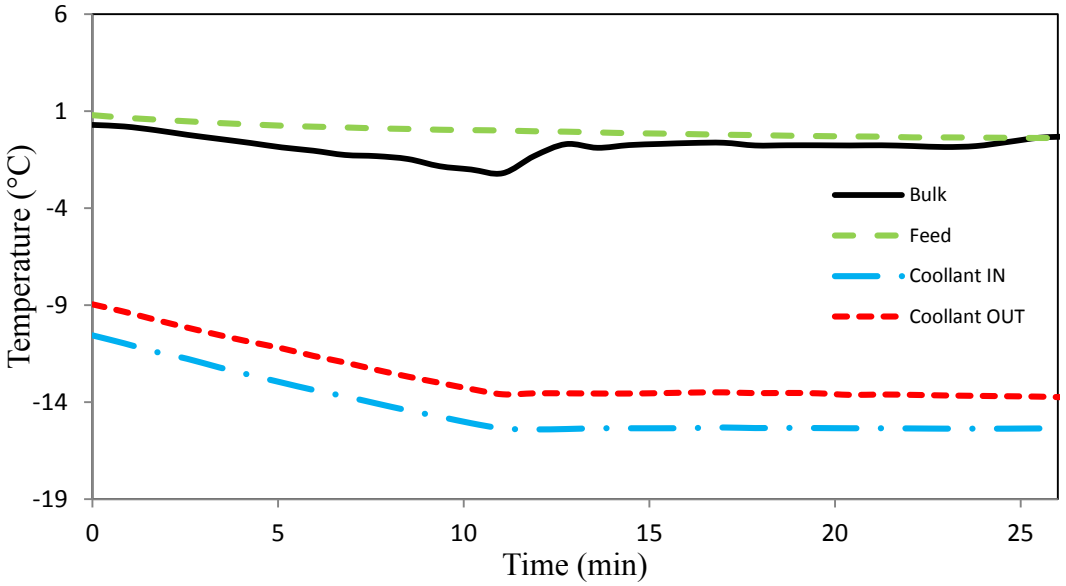

Figure A.4: Heat transfer driving force of 13.4 °C, scraper speed of 6.42 rpm

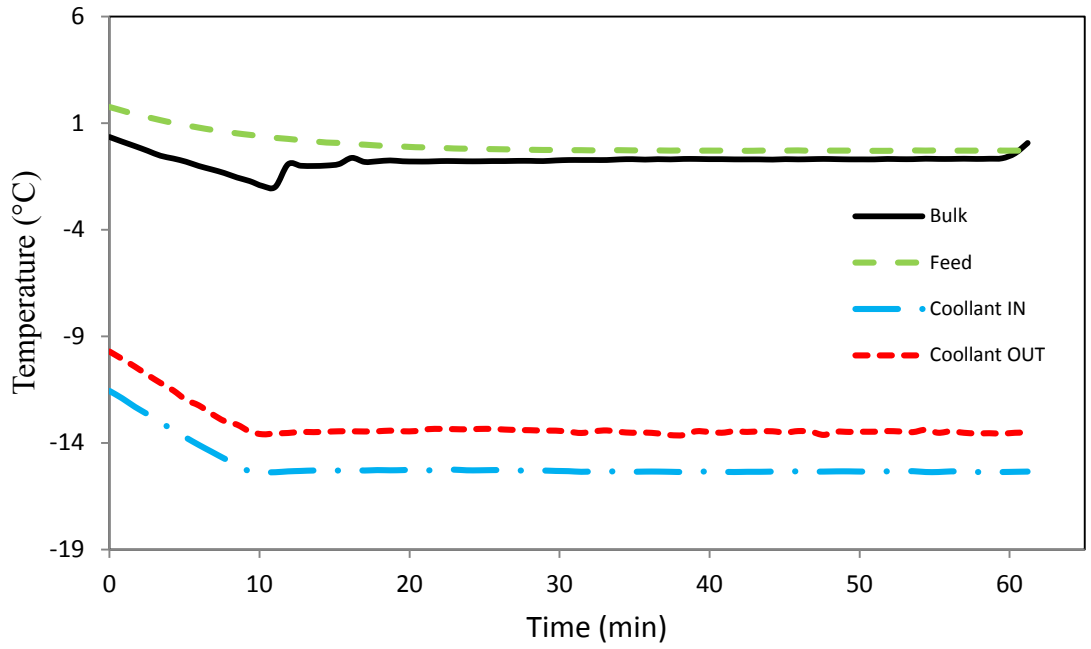

Figure A.5: Heat transfer driving force of 13.4 °C, scraper speed of 10.7 rpm

APPENDIX B

Calculation of average heat transfer rate during the induction time for an experimental run at a heat transfer driving force of 8.6 °C and a scraper speed of 10.7 rpm:

$$Q_{cm} = \dot{m} C_p \Delta T'$$

Specific mass flow rate of cooling medium: m = 0.486 kg/m^{2}s

Specific heat capacity of cooling medium at -10 °C: C_p = 1570 J/kg°C

$Qcm_{(average)}$ = 1087 W/m^2

Coollant IN	Coollant OUT	ΔTcm	Qcm
-9.92	-8.4	1.52	1160
-10.44	-8.81	1.63	1244
-10.51	-9.04	1.47	1122
-10.52	-9.11	1.41	1076
-10.45	-9.13	1.32	1007
-10.47	-9.13	1.34	1022
-10.45	-9.13	1.32	1007
-10.4	-9.12	1.28	977
-10.46	-9.11	1.35	1030
-10.43	-9.14	1.29	984
-10.43	-9.14	1.29	984
-10.45	-9.16	1.29	984
-10.43	-9.14	1.29	984
-10.46	-9.03	1.43	1091
-10.41	-9	1.41	1076
-10.43	-8.98	1.45	1106
-10.44	-8.98	1.46	1114
-10.43	-8.98	1.45	1106
-10.42	-8.99	1.43	1091
-10.43	-8.99	1.44	1099
-10.42	-9.01	1.41	1076
-10.43	-9.03	1.4	1068
-10.46	-9.01	1.45	1106
-10.4	-9.02	1.38	1053
-10.45	-9.02	1.43	1091
-10.44	-9.03	1.41	1076
-10.46	-9.03	1.43	1091
-10.43	-9.01	1.42	1083
-10.43	-9.03	1.4	1068
-10.42	-9.02	1.4	1068
-10.43	-9.02	1.41	1076
-10.45	-8.97	1.48	1129

-10.38	-8.99	1.39	1061
-10.4	-9.01	1.39	1061
-10.46	-8.99	1.47	1122
-10.44	-9.01	1.43	1091
-10.44	-9	1.44	1099
-10.45	-9	1.45	1106
-10.45	-9	1.45	1106
-10.42	-8.99	1.43	1091
-10.44	-8.99	1.45	1106
-10.44	-8.96	1.48	1129
-10.44	-8.97	1.47	1122
-10.45	-8.98	1.47	1122
-10.43	-9.02	1.41	1076
-10.43	-9	1.43	1091
-10.43	-9	1.43	1091
-10.44	-9.01	1.43	1091
-10.45	-9	1.45	1106
-10.42	-9.02	1.4	1068
-10.45	-9.02	1.43	1091
-10.46	-9	1.46	1114
-10.45	-9.01	1.44	1099
-10.45	-9.02	1.43	1091
-10.44	-9.02	1.42	1083
-10.41	-9.02	1.39	1061
-10.45	-8.99	1.46	1114
-10.43	-9.01	1.42	1083
-10.43	-9.01	1.42	1083
-10.43	-9	1.43	1091
-10.43	-9.03	1.4	1068
-10.43	-9.01	1.42	1083
-10.45	-8.99	1.46	1114
-10.44	-9	1.44	1099
-10.41	-8.99	1.42	1083
-10.43	-8.97	1.46	1114
-10.42	-8.98	1.44	1099
-10.45	-9.02	1.43	1091
-10.44	-9	1.44	1099
-10.44	-9.02	1.42	1083
-10.44	-9	1.44	1099
-10.43	-9.04	1.39	1061
-10.44	-9.04	1.4	1068
-10.42	-9.05	1.37	1045
-10.42	-9.04	1.38	1053
-10.43	-9.04	1.39	1061
-10.42	-9.04	1.38	1053
-10.45	-9.02	1.43	1091

-10.43	-9	1.43	1091
-10.45	-9.03	1.42	1083
-10.43	-9.04	1.39	1061
-10.44	-9.05	1.39	1061
-10.46	-9	1.46	1114
-10.46	-9.02	1.44	1099
-10.44	-9.03	1.41	1076
-10.44	-9.04	1.4	1068
-10.43	-9.02	1.41	1076
-10.44	-9.04	1.4	1068
-10.45	-9.01	1.44	1099
-10.45	-9.03	1.42	1083
-10.43	-9.01	1.42	1083
-10.4	-9.03	1.37	1045
-10.46	-9	1.46	1114
-10.42	-9.02	1.4	1068
-10.45	-9.09	1.36	1038
-10.4	-9.15	1.25	954
-10.4	-9.12	1.28	977